ICOSAHEDRAL ORDER IN METASTABLE METALLIC ALLOYS

Thesis by

Steven Mark Anlage

In Partial Fulfillment of the Requirements

for the Degree of

Doctor of Philosophy

California Institute of Technology

Pasadena, California

1988

(Submitted 23 October, 1987)

© 1988

Steven Mark Anlage

All Rights Reserved

For my Folks

The poets down here don't write noth'n at all,
They just stand back and let it all be.
Bruce Springsteen
Jungleland

ACKNOWLEDGEMENTS

My years at Caltech have been guided by the enthusiasm and insight of Professor W. L. Johnson. Bill has been a role model of the true physicist, someone who will solve any physical problem he sets his mind to. From him I have learned to appreciate all of solid state physics, from the most basic properties to the most practical applications.

I am also grateful to Art Williams who introduced me to the peculiar society in and around the Los Alamos National Laboratories. There I had the opportunity to work with one of the best theoretical physicists I have ever met, Darryl Smith. Later I also had the pleasure of working with and learning experimental skills from Ricardo Schwarz and other members of the Center for Materials Science.

Back at Caltech I had the good fortune to meet Eric Cotts. Eric has helped me through the most difficult times of my career and has become a very sincere friend. Along with Madeleine, Nathaniel and Susan, I became part of their family.

Everyday life at Caltech was made much more interesting, and sometimes rather turbulent, by my association with "the group." Professeur Duwez, Concetto Geremia, Angela Bressan and Joyce Ferrante kept us together and (usually) on speaking terms by means of the daily coffee hours. I spent hundreds of these coffee hours discussing life and work with fellow students, post-docs and professors (including P. Askenazy, M. Atzmon, D. Baxter, Y. T. Cheng, B. Dolgin, B. Fultz, L. Hazelton, R. Johnson, N. K. Mahale, W. J. Meng, A. Mutz, P. Pietrokowsky, K. Samwer, R. Schulz, K. Unruh, G. Wong, and X. Y. Yeh).

Life at Caltech is sometimes difficult. These difficulties have been smoothed out through my friendship with Ms. Susan Larson and the members of a certain J. Alfred Prufrock Society.

Funding for this work was provided for by the Eastman Kodak and International Business Machines Corporations as well as by the U.S. Department of Energy and the National Science Foundation.

ABSTRACT

We examine the consequences of short-range icosahedral order in metastable metallic alloys. There is evidence, both direct and indirect, for the existence of atomic clustering with icosahedral symmetry in supercooled liquid metals, metastable metallic alloys, and large-unit-cell intermetallic compounds. It is observed that a variety of metallic alloys can exhibit a long-range ordered structure with icosahedral point group symmetry upon rapid quenching from the liquid. We have carefully examined one of these icosahedral phase-forming systems in an effort to understand how the long-range ordered solid develops from the liquid phase. Our studies show that the icosahedral phase nucleates homogeneously from the liquid during the rapid quenching process.

We have developed a theory to explain qualitatively this observation. A model material is proposed, which is endowed with short-range icosahedral order broken up by defect structures. The thermodynamics of this model are described by a Ginzburg-Landau theory. The model displays a strong first-order phase transition from a high-temperature, heavily defected phase to a low-temperature phase with enhanced short-range icosahedral order. This transition is compared to our observations of icosahedral phase formation to fix the values of the theoretical parameters.

TABLE OF CONTENTS

	Page
ACKNOWLEDGEMENTS	iv
ABSTRACT	vi
LIST OF ILLUSTRATIONS	x
LIST OF TABLES	xv
I. Evidence of Icosahedral Ordering in Metals	
1. Introduction	1
1.1 Historical Overview	1
1.2 Evidence of Icosahedral Ordering in Liquid Metals	3
1.3 Evidence of Icosahedral Ordering in Intermetallic Compounds	6
1.4 Evidence of Icosahedral Ordering in Metallic Glasses	8
1.5 The Icosahedral Phase	12
II. Observations of Icosahedral Phase Formation	
2. Experimental Procedure	17
2.1 The Aluminum-Ruthenium Icosahedral Phase-Forming System	17
2.2 Sample Preparation	17
2.2a Alloy Preparation	18
2.2b Rapid Quenching	18
2.2c Mechanical Alloying	20
2.3 Sample Characterization	20
2.3a X-ray Diffraction	22
2.3b Differential Thermal Analysis	22
2.3c Atomic Absorption Spectroscopy	22

Page

2.3d Electron Microscopy 25

3. Experimental Results and Discussion 27

3.1 The Equilibrium Al-Ru Phase Diagram 27

3.2 The Nonequilibrium Al-Ru Phase Diagram 31

3.3 Ruthenium Segregation to the Icosahedral Grains 38

3.3a Sample Morphology 38

3.3b Ruthenium Segregation 41

3.4 Conclusions 42

III. A Theory of Icosahedral Phase Formation

4. The Predominantly Icosahedral Material 43

4.1 Icosahedral Short-Range Order and Icosahedral Phase Formation 43

4.2 The Physical Picture 43

4.3 Local Icosahedral Order Parameter 45

4.4 Disclination Lines 48

5. Thermodynamics of a Predominantly Icosahedral Material 55

5.1 Ginzburg-Landau Theory of Superconductivity 55

5.2 Ginzburg-Landau Theory of a Predominantly Icosahedral Material 57

5.3 The Discretized Theory 59

5.4 Phase Structure of the Predominantly Icosahedral Material 61

5.5 Results 65

6. Comparison of Theory and Experiment 69

6.1 Fixing the Theoretical Parameters 69

6.2 Summary and Conclusions 69

Page

Appendix I The Curved Space Description of Amorphous Materials 72

Appendix II A Field Theory of Local Icosahedral Order in Metals 75

A2.1 Physical Description 76

A2.2 Formal Description 77

A2.3 The Disorder Field 79

A2.4 Gauge Theories and the Free Energy Functional 82

REFERENCES 86

LIST OF ILLUSTRATIONS

Figure — Page

1.1 Clusters of atoms having the symmetry of the five Platonic solids. These are the a) tetrahedron, b) cube (hexahedron), c) octahedron, d) icosahedron and e) dodecahedron. 2

1.2 Two large unit cell intermetallic compound crystal structures. $Al_{12}Mo$ (top) has a BCC lattice with Mo atoms on the lattice sites surrounded by twelve Al atoms at the vertices of an icosahedron [after Walford, 1964]. $Mg_{32}(Al,Zn)_{49}$ (bottom) also has a BCC lattice with several shells of atoms in the basis having icosahedral symmetry [after Bergman et al., 1957]. 7

1.3 Five regular tetrahedra wrapped about a common edge do not close but instead leave a deficit angle of about 7° [after Nelson, 1983b]. 11

1.4 A set of electron diffraction patterns obtained from an icosahedral Al-Mn alloy by Shechtman et al. The accompanying stereographic projection of the icosahedral point group shows that the rotation angles between high symmetry diffraction axes exactly match those of an icosahedron [after Shechtman et al., 1984]. 13

2.1 Schematic diagram of the piston and anvil rapid quenching apparatus. A metal charge is melted by RF heating in a fused silica crucible and allowed to drop vertically. When the drop interrupts 19

Figure Page

the light beam, the trigger, D, allows the piston, B, to meet the anvil, A, just as the drop arrives [after Mehra, 1984].

2.2 The Spex 8000 Mixer Mill used for mechanical alloying experiments. A hardened steel canister containing Al-Ru powder and six hardened steel balls is shaken in an irregular figure eight motion by means of a motor [after Spex Industries]. 21

2.3 The Philips vertical goniometer used for x-ray analysis of rapidly quenched Al-Ru alloys. An x-ray tube anode line source produces an incident beam through divergence Soller slits to illuminate the specimen. The Bragg diffracted beam leaves the specimen at the angle of incidence and proceeds through a receiving Soller slit to the detector [after Philips Corporation]. 23

2.4 An x-ray diffraction pattern of a piston and anvil quenched $Al_{86}Ru_{14}$ alloy. The diffraction peaks can be indexed to an Al-Ru solid solution (sharp peaks) and icosahedral Al-Ru (broad peaks). The icosahedral phase diffraction peaks are labelled with the indexing convention of Bancel et al. [Bancel et al., 1985]. 24

3.1 Equilibrium phase diagram for the Al-rich end of the Al-Ru system. Solid symbols represent measured values. 28

3.2 A scanning electron micrograph showing Al_6Ru crystals in the as-cast $Al_{80}Ru_{20}$ alloy. 29

Figure		Page
3.3	A scanning electron micrograph showing $Al_{13}Ru_4$ (faceted crystal in center) in the as-cast $Al_{80}Ru_{20}$ alloy.	30
3.4	A scanning electron micrograph showing the structure of an $Al_{90}Ru_{10}$ ingot after cooling in the calorimeter at the rate of 1 K/min. Peritectic formation of Al_6Ru is evident at the boundary between $Al_{13}Ru_4$ and the Al-rich matrix.	32
3.5	Schematic piston and anvil non-equilibrium liquid quenching phase diagram for the $Al_{1-x}Ru_x$ system for $x < 25$ at% Ru. Dotted lines indicate the equilibrium phase structure as determined by Anlage et al. [Anlage et al., 1987]. Vertical dotted lines show the Al_6Ru and $Al_{13}Ru_4$ phases. A dotted region in the upper right corner shows equilibrium between another Al-Ru compound and the liquid phase.	34
3.6	Schematic Gibbs free energy versus Ru composition for liquid Al-Ru, icosahedral Al-Ru, and $Al_{13}Ru_4$. The icosahedral phase begins to form peritectically at $T = T_p$.	37
3.7	Bright field image from piston and anvil quenched $Al_{90}Ru_{10}$ showing the rosette shaped icosahedral particles surrounded by aluminum matrix. An arrow shows the approximate location where the fivefold diffraction pattern (inset) was obtained.	39

Figure		Page
3.8	Bright field image from piston and anvil quenched $Al_{97.5}Ru_{2.5}$ showing the equi-axed icosahedral particles surrounded by an aluminum matrix.	40
4.1	Schematic physical picture of the predominantly icosahedral material. Regions of high local icosahedral order are separated by linear defect structures.	44
4.2	Polytope $\{3,3,5\}$ seen in an exploded view as a series of 3-dimensional cuts through the 4-dimensional sphere S^3 (represented as a semicircle on the left). As the fourth coordinate, z, varies from 2 to 0, the cuts reveal a point (z=0), an icosahedron (z=τ), a dodecahedron (z=1), a larger icosahedron (z=τ^{-1}), and an icosidodecahedron (z=0).	47
4.3	An icosahedral cluster of atoms and the Voronoi construction for the central atom.	49
4.4	The three types of nearest-neighbor bonds; 0°, -72° (extra tetrahedron inserted around the bond) and +72° (missing tetrahedron) disclinations [after Nelson, 1983b].	51
4.5	The Kasper polyhedra (CN14, CN15, CN16) and Bernal holes (CN10, CN9, CN8) along with their representation in terms of disclination lines [after Nelson, 1983b].	52

Figure		Page
4.6	The A15 (A_3B) structure with disclination lines running through the A atoms in three mutually perpendicular directions [after Sinha, 1972].	54
5.1	Comparison of the type II superconductor and a predominantly icosahedral material.	56
5.2	Cyclic annealing treatment of a 16^3 lattice with only disclination lines present. The internal energy of the disclination lines (in units of E_l) is plotted against the dimensionless inverse temperature E_l/k_BT.	64
5.3	Disclination line internal energy (in units of E_l) is plotted against Monte Carlo update number for a 16^3 lattice with only disclination lines on the links. These annealing treatments are carried out both above and below the transition temperature.	66
A2.1	a) A closed plane curve C which surrounds a line defect in the predominantly icosahedral material. b) A discretized version of the closed plane curve C. The order parameter is defined on the sites i, j, etc., and the frustration field transporters, U_{ij}, etc., exist on the line segments between sites.	80

LIST OF TABLES

Table		Page
5.1	The formal analogy between the Ginzburg-Landau theory of superconductivity and the gauge field theory of predominantly icosahedral materials (PIM).	58
5.2	Values of the energy per unit length of all disclination lines used in the Monte Carlo simulations.	62

I. Evidence of Icosahedral Ordering in Metals

Chapter 1 Introduction

1.1 Historical Overview

Until quite recently, little serious consideration has been given to the possibility of atomic clustering with icosahedral symmetry in condensed matter. The icosahedron is one of the five Platonic solids illustrated in Figure 1.1. Because these five solids are the only regular polyhedra in three dimensions, Plato used them as the basis of his natural philosophy [Weyl, 1952]. It is interesting to note that despite the later belief that icosahedral symmetry is inconsistent with crystallography, the abstract notion of a dodecahedron (Figure 1.1e) was first inspired by the shapes of pyrite crystals found by the ancient Greeks in Sicily [Weyl, 1952].

The symmetry group of the icosahedron includes twelve fivefold rotation axes passing through its opposite vertices. In classical crystallography, which assumes that all structures can be built up by a periodic tesselation of space with a single unit cell, global fivefold symmetry axes are impossible [Hamermesh, 1962; Kittel, 1976; Burns, 1985]. This fact is related to the observation that regular tetrahedra and icosahedra cannot be used to tesselate space without overlapping or leaving gaps [Zallen, 1983]. For this reason, the mainstream of condensed matter research has flowed away from consideration of fivefold and icosahedral symmetries in metallic systems.

Despite the belief that icosahedral symmetry was not considered possible in metallic crystals, a number of workers maintained that small clusters of atoms with this symmetry could be found in liquid metals, intermetallic compounds and metallic glasses. This short-range clustering comes about because the icosahedron represents the highest local density and the lowest possible local energy structure for twelve atoms in contact with one [Frank, 1952]. Frank believed that icosahe-

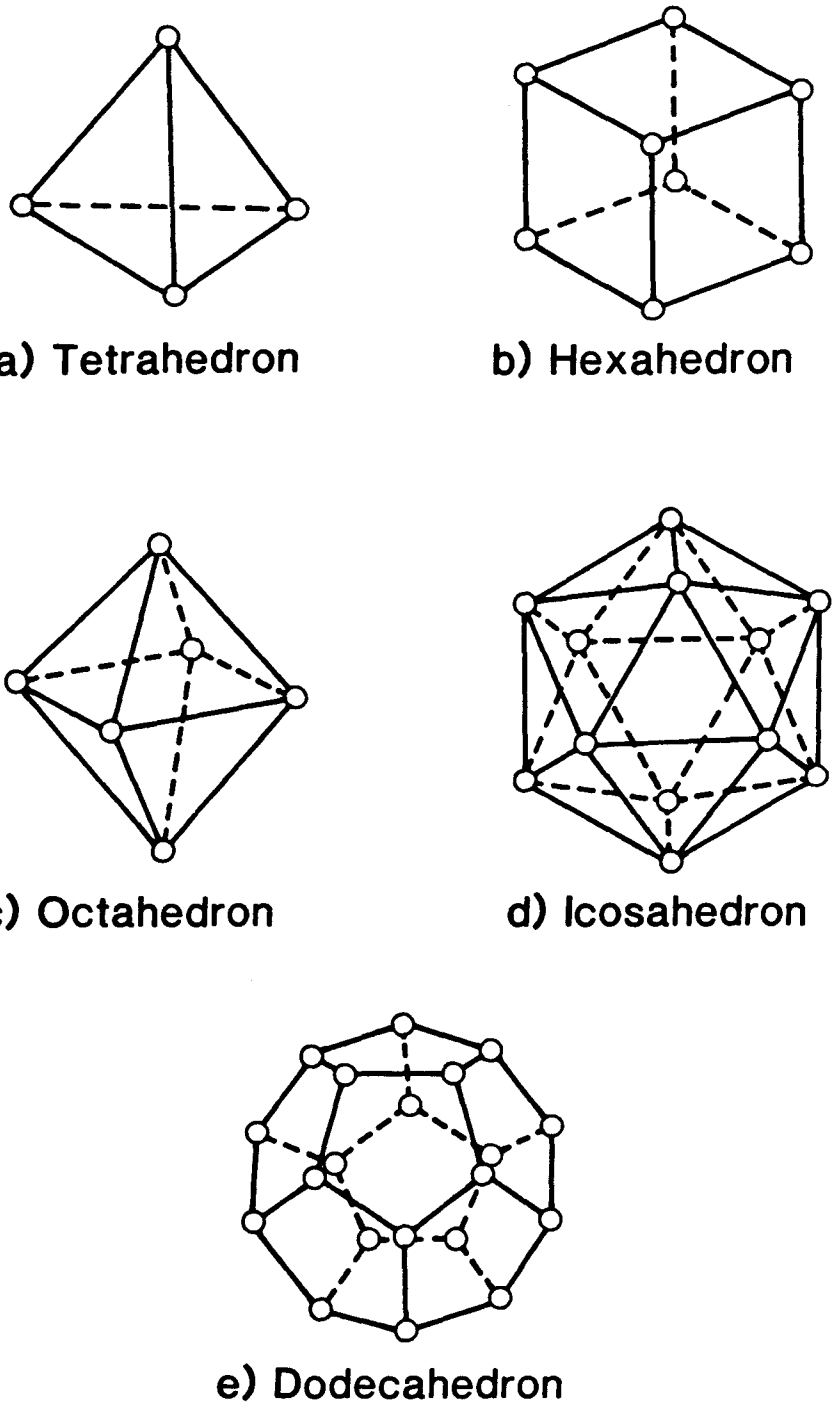

Figure 1.1 Clusters of atoms having the symmetry of the five Platonic solids. These are the a) tetrahedron, b) cube (hexahedron), c) octahedron, d) icosahedron and e) dodecahedron.

dral groupings of atoms present nucleation barriers for crystallization of ordinary close-packed structures; hence, they are responsible for the extreme supercooling properties frequently observed in elemental liquid metals [Turnbull, 1950; Perepezko and Paik, 1984]. The pioneers of x-ray crystallography discovered that many intermetallic compounds have a large unit cell and basis. In performing structural refinements of these crystals, they found that many clusters of atoms in the basis have local icosahedral symmetry [Pauling, 1960; Samson, 1968; 1969]. Sadoc, Kléman and Nelson have developed a successful theory of metallic glass structure based on a frustrated packing of icosahedral clusters of atoms [Sadoc, 1981; Kléman and Sadoc, 1979; Nelson and Widom, 1984].

All of this work went relatively unnoticed until the tranquil world of crystallography was shaken to its foundations by the discovery of a rapidly quenched aluminum-manganese alloy, which diffracts electrons with icosahedral point group symmetry [Shechtman et al., 1984]. This novel material, known as the icosahedral phase, has since been found in many other metastable alloys as well as in several equilibrium systems (a list is presented in Section 1.5). Although the atomic structure of this material has not yet been determined, it is a fundamental hypothesis of this work that icosahedral clustering plays a significant role in the formation and structure of the icosahedral phase.

In the rest of this chapter we shall briefly review the accumulated evidence (both direct and indirect) of icosahedral ordering in metallic systems. Our objective is to show that icosahedral clustering is an important structural motif in certain liquid metals, intermetallic compounds and metallic glasses.

1.2 Evidence of Icosahedral Ordering in Liquid Metals

Metallic bonding favors configurations of atoms in which the number of nearest-neighbors around a given atom is maximized [Pauling, 1960]. The bonding properties of metallic atoms are nearly isotropic, so the atom can be profitably modeled as

a sphere of some appropriate radius. The maximum number of equal size spheres that can be in contact with a given sphere is twelve [Frank, 1952]. Locally, this can be achieved in three different ways: face-centered cubic (FCC) packing, hexagonal close-packing (HCP) and an icosahedral cluster. Frank has noted that an icosahedral grouping of thirteen atoms interacting through a Lennard-Jones potential has a binding energy 8.4% less than similarly sized clusters of face-centered cubic or hexagonal close-packing [Frank, 1952].

Hoare and Pal [Hoare and Pal 1971; Hoare, 1976] have calculated the minimum energy structures of finite clusters of atoms interacting by central, two-body, Lennard-Jones interactions. They find that such clusters tend to grow in one of three modes: tetrahedral, pentagonal or icosahedral, rather than as FCC or HCP clusters. None of these minimum energy growth modes can be continued indefinitely to fill all space (they suffer from "self-limiting growth" [Hoare, 1976]), so the clusters are referred to as "anticrystalline." This topological frustration (i.e., the inability to fill space with a minimum energy configuration) gives rise to interesting effects when materials are constrained to adopt such growth modes in favor of crystalline growth. For instance, Tammann [see Hoare, 1976] has proposed that the rise in viscosity accompanying the glass transition in a supercooled liquid is due to the growth and mutual impingement of anticrystalline units in the liquid.

Farges [Farges, 1973] has carried out experiments in which jets of inert gas are allowed to expand into a vacuum, and the resulting clusters of atoms are analyzed by electron diffraction. These results show that 500 atom clusters consist of a non-crystalline core (of the same size as the clusters calculated by Hoare and Pal [Hoare and Pal, 1971]) surrounded by an FCC cluster of the rare gas atoms. Thus, it appears that noncrystallographic clustering is preferred, up to a certain cluster size, in atom-by-atom growth processes. Harris et al. [Harris et al., 1984] have carried out experiments in which jets of inert gas are allowed to expand into a vacuum

and the sizes of the resulting clusters of atoms are analyzed. It is found that the clusters tend to have sizes corresponding to a few "magic numbers" of atoms. These magic numbers correspond closely to particularly stable "anticrystalline" clusters of Lennard-Jones atoms calculated by Hoare and Pal [Hoare and Pal, 1971]. The "magic number" clusters have noncrystallographic symmetries based on one or more shells of icosahedral or dodecahedral coordination.

A number of investigators have observed a variety of prefreezing phenomena in liquid metal systems. Turnbull [Turnbull, 1950] and Perepezko and Paik [Perepezko and Paik, 1984] have supercooled elemental liquid metals (by eliminating heterogeneous nucleation sites) to 30-40% of the absolute melting temperature before crystallization begins by homogeneous nucleation. This deep excursion into the metastable regime implies the existence of relatively stable structures (at least more stable than crystalline nuclei) in the supercooled liquid. With these observations in mind, Frank [Frank, 1952] proposed that icosahedral clustering in the supercooled liquid metal is responsible for the deep supercooling. The icosahedral cluster is a low energy structure; its topological short-range order is somewhat different from that of FCC or HCP crystals. The atomic rearrangements required to transform the cluster into one of the common crystal packings are energetically costly and can be overcome only when they are done on long length scales. This requires a substantial structural fluctuation, which is likely to occur only at a certain degree of supercooling (in the absence of a seed crystal). In other words, icosahedral clustering presents a nucleation barrier for crystallization of the liquid metal, thus explaining the observed supercooling properties.

Ubbelohde notes that the specific heat C_p of many metallic melts increases as the substance is cooled toward the melting temperature [Ubbelohde, 1965]. He attributes this rise to increasing formation of "anticrystalline" clusters in the liquid. Since anticrystalline clusters are energetically more stable than small FCC or HCP

clusters, the excess enthalpy released shows up as an increase in C_p.

The picture of a liquid metal can be summarized as follows. One can think of a supercooled liquid metal (with heterogeneous nucleation sites for the close-packed crystalline phases removed) as a system with both crystalline and anti-crystalline nuclei forming at their respective nucleation frequencies. Depending upon the material, the driving force (i.e., degree of supercooling) will eventually favor the growth of a solid phase from one of the two types of nucleation sites. The solid phase that nucleates and grows will be either crystalline or quasi-crystalline, depending upon the growth kinetics. In cases of extreme and rapid supercooling, the liquid structure (with both crystalline and anticrystalline local order) will be frozen in, and the resulting solid is a metallic glass.

1.3 Evidence of Icosahedral Ordering in Intermetallic Compounds

It is known that many intermetallic crystal structures have large unit cells with many atoms in the basis [Samson, 1968]. To simplify the structural refinement of these crystals, Samson has developed a technique to represent the crystal basis as a packing of coordination polyhedra [Samson, 1969]. One of the most common coordination polyhedra in intermetallic compounds is that of coordination twelve, isomorphic to the icosahedron. Samson has identified several other common coordination polyhedra involving higher coordinations [Samson, 1969]. These include the Friauf polyhedra (coordination number (CN) 16), the $\mu-$phase polyhedra (CN 15), the hexagonal prism and antiprism (CN 14) and a few other irregular polyhedra.

Several representative large unit cell crystal structures are shown in Figure 1.2. The $Al_{12}Mo$ crystal structure [Walford, 1964] (Figure 1.2 (top)) consists of a molybdenum atom at each body-centered cubic lattice site surrounded by an icosahedral cluster of twelve aluminum atoms. An example of more extensive icosahedral clustering is the crystal structure of $Mg_{32}(Zn, Al)_{49}$ [Bergmann et al., 1957] shown in Figure 1.2 (bottom). This crystal also has a body-centered cubic lattice with an

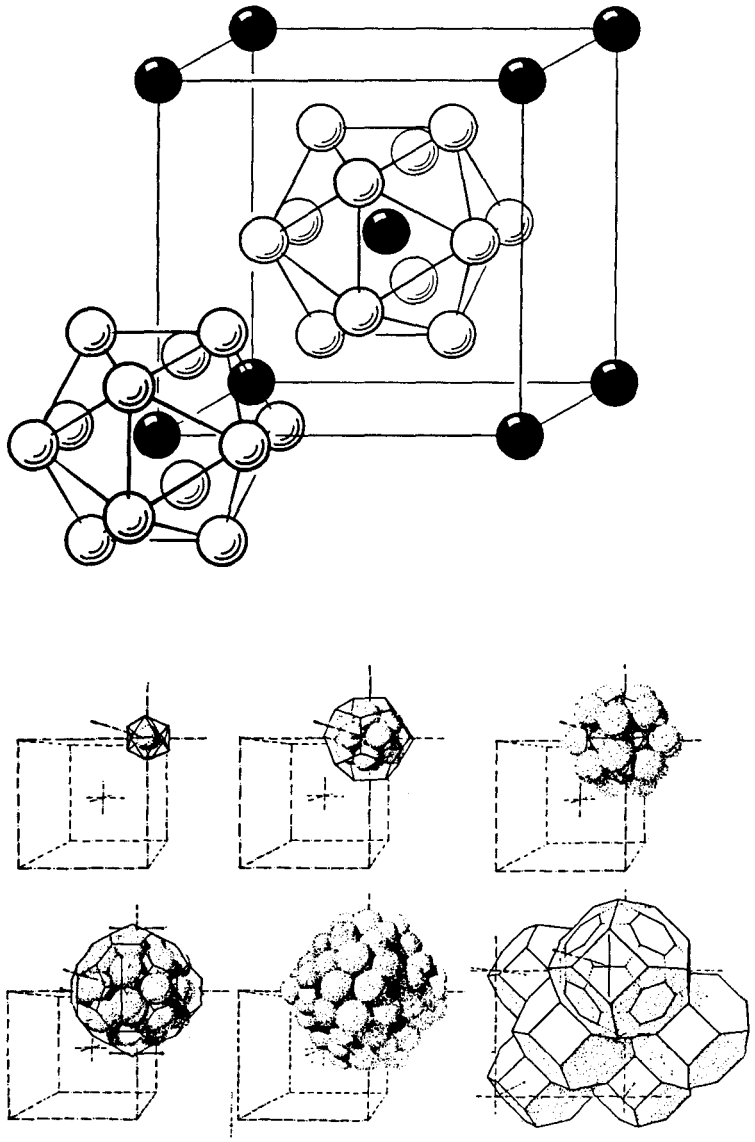

Figure 1.2 Two large unit cell intermetallic compound crystal structures. $Al_{12}Mo$ (top) has a BCC lattice with Mo atoms on the lattice sites surrounded by twelve Al atoms at the vertices of an icosahedron [after Walford, 1964]. $Mg_{32}(Al,Zn)_{49}$ (bottom) also has a BCC lattice with several shells of atoms in the basis having icosahedral symmetry [after Bergman et al., 1957].

atom *on each lattice site*. Surrounding that atom are shells of atoms that sit on the vertices of an icosahedron, a larger dodecahedron, a still larger icosahedron and a final shell of atoms making up a truncated icosahedron with tetrahedral symmetry. It is interesting to note that the icosahedral phase is found in samples of rapidly solidified liquids with composition $Al_{12}Mo$ and $Mg_{32}(Zn, Al)_{49}$.

Examination of these and many other intermetallic compounds lead one to the following conclusion. When atoms are in the basis of a large unit cell metallic crystal (hence relatively free of crystallographic constraints), they may cluster into units having noncrystallographic symmetry. The fact that these noncrystallographic groupings are predominant in the basis is a reflection of their stability and simplicity. This is yet another reason why icosahedral clustering must be taken seriously in any theory of the structure of metals.

1.4 Evidence of Icosahedral Ordering in Metallic Glasses

Bernal's [Bernal, 1965] dense random packing of hard spheres was an early attempt to model the structure of a monatomic metallic glass. This model includes the qualitative features of a metallic glass with an isotropic, purely repulsive pair interaction. Since the model has no attractive term in the interaction potential, one does not expect to find an abundance of the low energy tetrahedral and icosahedral clusters in the structure. To go beyond these simplistic hard sphere packing models, a number of researchers have modeled the glassy state with more sophisticated interaction potentials by means of computer simulated quenches from the molten state. The structures resulting from the simulations can be used to calculate the diffraction pattern that is then compared directly with experiment. These simulations also reveal a great deal of microscopic information about the metallic glass structure.

Briant and Burton [Briant, 1976; Briant and Burton, 1978] have performed molecular dynamics simulations of a model monatomic liquid interacting through

a *Lennard-Jones* potential. During a rapid quench of these computer liquids, they have observed icosahedral clustering in groups of thirteen and 55 atoms. They come to the conclusion that icosahedral clusters are quite prominent in metallic glasses for the following reasons: (i) A similarity in the scattering structure factor of amorphous metals and the thirteen-atom icosahedral cluster, (ii) The direct observation of icosahedral clusters in his computer simulated glasses, and (iii) The ability of icosahedral clusters to form in atom-by-atom growth processes (e.g., thin-film evaporation) because of their energetic stability.

To extract more information from these computer simulations of monatomic Lennard-Jones liquids, Steinhardt, Nelson and Ronchetti [Steinhardt et al., 1981; 1983] defined a set of bond orientational order parameters. Every nearest-neighbor bond, with a midpoint at $\vec{r}$, makes angles $\theta(\vec{r})$ and $\phi(\vec{r})$ with respect to some fixed global direction. The value of the order parameter is given by the set of numbers,

$$Q_{lm}(\vec{r}) \equiv Y_{lm}(\theta(\vec{r}), \phi(\vec{r})), \tag{1.1}$$

where Y_{lm} are the (three-dimensional) spherical harmonics, with $-l \leq m \leq l$. Since $Q_{lm}(\vec{r})$ is not rotationally invariant, i.e., it depends on the choice of fixed global direction, Steinhardt et al. defined the quantity,

$$Q_l(\vec{r}) \equiv \sqrt{\frac{4\pi}{2l+1} \sum_{m=-l}^{l} |\langle Q_{lm}(\vec{r}) \rangle|^2}, \tag{1.2}$$

where $\langle Q_{lm}(\vec{r}) \rangle$ denotes the average of $Q_{lm}(\vec{r})$ over all the bonds in a given volume of the sample.

Systems with cubic rotational symmetry have large values of Q_4 whereas those with icosahedral clustering show large values of Q_6 [Steinhardt et al., 1981; 1983]. Steinhardt et al. evaluated these order parameters for a supercooled Lennard-Jones liquid and noted a dramatic increase in the value of Q_6, and a much more modest increase in Q_4, during the quench. The observed increase in the icosahedral bond-

orientational order parameter began a flurry of activity in the theory of metallic glasses.

Nelson [Nelson, 1983a; 1983b], building on the ideas of Kléman [Kléman and Sadoc, 1979] and Sadoc [Sadoc, 1981], later proposed that supercooled liquid metals and metallic glasses can be thought of as systems with defective icosahedral bond orientational order. This theory predicts a scattering structure factor in close agreement with those obtained experimentally on elemental amorphous thin metal films [Sachdev and Nelson, 1984; 1985]. Like most other theories of disordered systems, Nelson's metallic glass model rests on the concept of frustration [Toulouse, 1977]. As we see in Figure 1.3, five perfect tetrahedra wrapped around a common edge will leave a deficit angle of about 7°. If one assigns atoms to each of the vertices in this figure, it is clear that one of the atoms will not be in the potential energy minimum of all of its neighbors (in fact, it has two equivalent choices). This local topological frustration is responsible for the global topological disordering in a material with atoms that prefer local tetrahedral coordination.

All of the computer simulations discussed above have been performed on model monatomic systems. Yet, it is known that all metallic glasses that are stable at room temperature are made up of two or more elements. To address the problem of alloy glasses, Hafner has constructed realistic computer models of the simple metal glasses $Ca_{70}Mg_{30}$ and $Mg_{70}Zn_{30}$ and has evaluated their bond angle distribution functions [Hafner, 1982; 1985]. This function $f(\theta)$ represents the probability that the directions from a central atom to two of its neighbors form an angle θ. By examining this function for the metallic glasses studied, Hafner concludes that there are a large number of near-icosahedral and defected icosahedral coordinations in their structures [Hafner, 1982; 1985].

At the moment, computer simulations provide the only direct evidence for noncrystallographic clustering in metallic glasses. Despite this, the idea that a

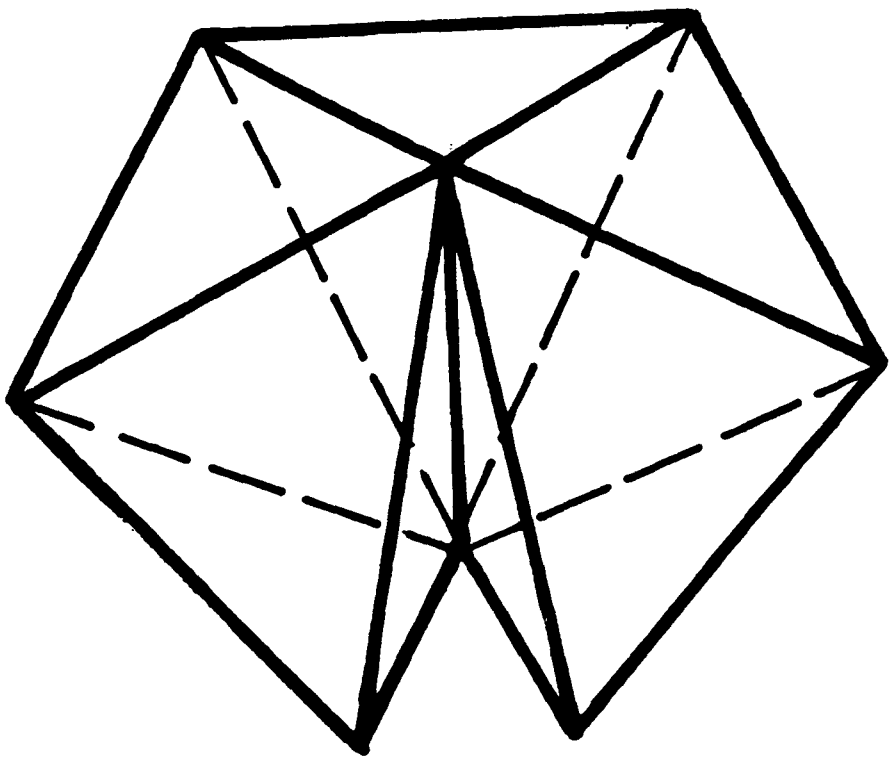

Figure 1.3 Five regular tetrahedra wrapped about a common edge do not close but instead leave a deficit angle of about 7° [after Nelson, 1983b].

frustrated packing of icosahedral units is responsible for metallic glass formation has proven to be very fruitful.

In summary, Sections 1.2-1.4 have shown that when atoms in a metal are free from crystallographic constraints (e.g., in the basis of a large unit cell intermetallic compound, in a liquid metal, or in a metallic glass), they tend to group into low energy noncrystallographic clusters. This structural motif must be taken into consideration if one wants to understand the structure and dynamics of noncrystalline metals.

1.5 The Icosahedral Phase

Direct experimental evidence of the existence of long-range icosahedral order in condensed matter came with the discovery by Shechtman et al. [Shechtman et al., 1984] of the icosahedral phase. This phase is remarkable because it diffracts electrons with the point group symmetry of an icosahedron (see Figure 1.4). This point group is unique in condensed matter, and because of its global fivefold symmetry, it is inconsistent with the tenet of classical crystallography, which states that a perfect crystal is made up of a periodic tiling of a single packing unit.

The icosahedral phase was originally discovered in a rapidly quenched binary alloy of composition $Al_{86}Mn_{14}$. It has been found subsequently in rapidly quenched binary Al-(Cr, V, Mo, Ru, W, Re) alloys [Bancel and Heiney, 1986], $Pd_{60}U_{20}Si_{20}$ [Poon et al., 1985], Ni-Ti-V [Zhang et al., 1985], Fe-Ti [Dong et al., 1986], Al-Cu-Li [Ball and Lloyd, 1985], $Mg_{32}(Al,Zn)_{49}$ [Ramachandrarao and Sastry, 1985] and V-Ni-Si [Kuo et al., 1987]. The icosahedral phase appears to be an equilibrium peritectic compound in the Al-Cu-Li, Al-Cu-Mg, Al-Zn-Li and Al-Zn-Mg ternary systems [Cassada et al., 1986].

Several models have been proposed for the atomic structure of the icosahedral phase. Levine and Steinhardt [Levine and Steinhardt, 1984] propose that the icosahedral phase is a quasi-crystal composed of two distinct unit cells with special

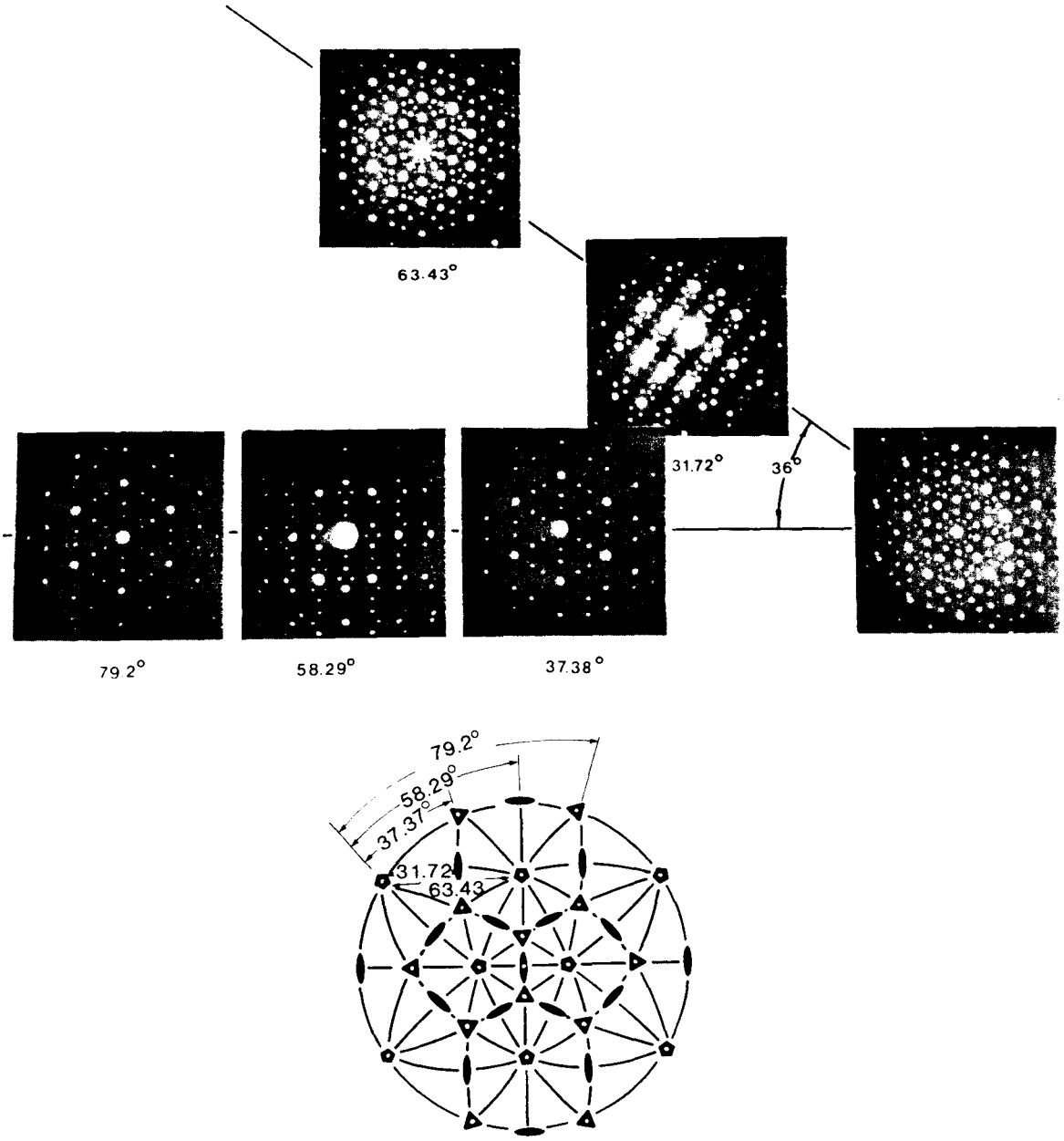

Figure 1.4 A set of electron diffraction patterns obtained from an icosahedral Al-Mn alloy by Shechtman et al. The accompanying stereographic projection of the icosahedral point group shows that the rotation angles between high symmetry diffraction axes exactly match those of an icosahedron [after Shechtman et al., 1984].

relationships between their edges that produce long-range icosahedral orientational order. Socolar et al. [Socolar et al., 1985] have proposed a generalized crystallography in which all non-crystallographic symmetries can be accommodated with the use of quasi-periodic tilings of two appropriately chosen unit cells.

An alternative structural model of the icosahedral phase has been proposed by Stephens and Goldman [Stephens and Goldman, 1986]. In their model, the icosahedral phase is a "glassy" agglomerate of icosahedral units (clusters) that join up face-to-face or vertex-to-vertex so as to preserve long-range orientational order between icosahedra. Because of topological frustration, these icosahedral units do not fill space, so there is translational disorder as well as a need to introduce interstitial (primarily octahedral) groupings of atoms to fill in the gaps. Both the icosahedral quasi-crystal and icosahedral glass models reproduce the electron diffraction experiments of Shechtman et al. [Shechtman et al., 1984].

Pauling [Pauling, 1985] has proposed a third model for the structure of the icosahedral phase. He suggests that a twentyfold twin of a large unit cell cubic crystal is responsible for the observed electron diffraction patterns. Pauling later suggested that a very large unit cell crystal with extensive icosahedral order in the basis can produce pseudo-icosahedral electron diffraction patterns [Pauling, 1987]. A series of experiments, including dark-field [Shechtman and Blech, 1985] and high-resolution [Hiraga et al., 1985] transmission electron microscopy imaging, high-resolution x-ray diffraction [Bancel et al., 1985] and convergent beam electron diffraction [Bendersky and Kaufman, 1986] are all inconsistent with Pauling's models. All of the accumulated experimental evidence on the icosahedral phase suggests that it is a true noncrystallographic state of solid matter (i.e., the symmetry of this material is not among the 230 known space groups for crystals).

There are several interesting problems that have not yet been solved concerning the icosahedral phase. First, the atomic structure of the icosahedral phase has yet to

be determined. This has not been done because the techniques of traditional crystallography are of little value when dealing with quasi-periodic structures. Initially it was not even clear if a quasi-periodic structure could produce a diffraction pattern with sharp and distinct peaks, as is observed in x-ray, electron and neutron diffraction experiments. Since sets of parallel diffracting planes of all possible d-spacings can be found in quasi-periodic structures, it would appear that reciprocal space is completely filled with diffraction spots. The resolution of this dilemma comes from considering the three-dimensional, quasi-periodic structure as a projection of a six-dimensional simple cubic lattice onto an appropriately oriented three-dimensional hyperplane [Kramer and Neri, 1984]. A similar projection is made in reciprocal space, where it is found that the best fit to experimental data occurs when the structure factor associated with a diffraction spot decreases exponentially with its projection distance [Elser, 1986]. A complete calculation of the diffraction intensity requires knowledge of the atomic basis associated with each quasi-lattice site. So far, it has proven impossible to find the correct basis [Bak, 1986].

A second set of interesting problems concerns a comparison of the physical properties of amorphous, icosahedral and crystalline materials at the same composition. For instance, we would like to know if any new collective phenomena (e.g., phonons, superconductivity, and magnetism) are associated with the unique point group symmetry and structure of the icosahedral phase. We have performed electrical resistivity measurements of icosahedral, amorphous and crystalline aluminum-ruthenium thin films between 4.2K and room temperature [Anlage et al., 1987]. We find that the magnitude and temperature dependence of the resistivity of icosahedral Al-Ru is most similar to that of amorphous Al-Ru and distinctly different from that of crystalline Al-Ru at the same composition.

A third question of interest concerns how and why the icosahedral phase forms from the liquid, vapor, or solid states. Understanding the formation conditions will

allow one to predict which alloys will display the icosahedral phase and give some clues about their atomic structure and properties.

This thesis is devoted primarily to the third question. In Part II we shall discuss experimental work on a particular icosahedral phase-forming system: the binary alloys of aluminum and ruthenium. From this study we come to the conclusion that the icosahedral phase nucleates homogeneously from the rapidly supercooled Al-Ru liquid. In Part III we consider the thermodynamics of a model material that is endowed with icosahedral short-range order. Since we have seen that icosahedral clustering is a structural motif in certain metals, it is of interest to see if that kind of ordering can be extended to a global scale. It is shown that this predominantly icosahedral material can display a phase with enhanced short-range icosahedral orientational order. This phase is separated from a high-temperature, heavily defected phase by a strong first order phase transition. We compare this phase transition to the liquid-to-icosahedral phase transition produced during the rapid quenching experiments discussed in Part II and use some of our experimental results to fix the parameters in the theory.

II. Observations of Icosahedral Phase Formation

Chapter 2 Experimental Procedure

In this chapter we discuss the techniques used to prepare and characterize samples containing the icosahedral phase. We have concentrated this experimental effort upon the aluminum-ruthenium icosahedral phase-forming system.

2.1 The Aluminum-Ruthenium Icosahedral Phase-Forming System

Of the many icosahedral phase-forming systems mentioned in Section 1.5, we have chosen one to study in detail. The binary Al-(Mn,Cr,Fe) are the most frequently studied systems. Since we were initially interested in studying the superconducting properties of the icosahedral phase, the presence of 3d transition metals posed the problem of magnetic moment formation at low temperatures. For this reason the Al-Ru binary system was chosen, Ru being a 4d transition metal, not prone to isolated moment formation.

From a metallurgical point of view the Al-Ru system is simpler than the Al-Mn system. In Section 3.1 we shall see that the Al-Ru system has relatively few equilibrium phases that compete for formation with the metastable icosahedral phase. The same region of the equilibrium Al-Mn phase diagram has five intermetallic phases [Taylor, 1960]. Hence, the Al-Ru icosahedral phase has proven relatively easy to form. We have prepared the Al-Ru icosahedral phase by means of liquid quenching [Anlage et al., 1987a], mechanical alloying [Anlage and Schwarz, 1987b] and in thin film form [Anlage et al., 1987c].

2.2 Sample Preparation

For the phase diagram studies discussed in Chapter 3, bulk ingots of various compositions were produced. In this section we describe the alloying and rapid quenching techniques used to prepare the samples.

2.2a Alloy Preparation

Ingots were produced by starting with high purity elemental metals. The ruthenium was initially in powder form, 99.95% pure (obtained from the Johnson-Matthey Company). To deoxidize this material, the powder was statically compressed into pellets. The pellets were then placed onto a water-cooled "silver boat" enclosed in a high purity argon atmosphere. Induction heating was used to simultaneously heat the ruthenium pellets and a piece of high purity zirconium, placed on the silver boat a few inches away. After this treatment, the ruthenium pellet changed from a dark gray to a silver gray color.

The 99.999% pure aluminum (obtained from the Johnson-Matthey Company) in the form of rods, 0.25 inches in diameter, was etched in a 90% HNO_3, 10% HF solution to remove the surface oxide layer just prior to alloying. In the equilibrium phase diagram study, the Ru and Al were placed in an alumina crucible, which was heated in an electrical furnace inside a glove box containing argon gas. A dynamic purification system circulated the argon gas at a rate of 40 cubic feet per minute and maintained partial pressures of O_2 and H_2O at levels below 1 part per million. The alloy casts were slowly cooled in the furnace.

In the non-equilibrium phase diagram study, the elements were placed in an alumina crucible enclosed in a high purity (99.9999% pure) static argon atmosphere. The elements were then heated inductively until they were alloyed.

2.2b Rapid Quenching

Rapid quenching of a liquid was first used to produce bulk amorphous metallic alloys by Klement et al. [Klement et al., 1960]. Later, Pietrokowsky [Pietrokowsky, 1963] developed the piston and anvil technique to rapidly solidify drops of molten metal (see Figure 2.1). In this apparatus, an alloy charge is first melted inductively in a fused silica crucible. The liquid metal falls as a drop and interrupts a light

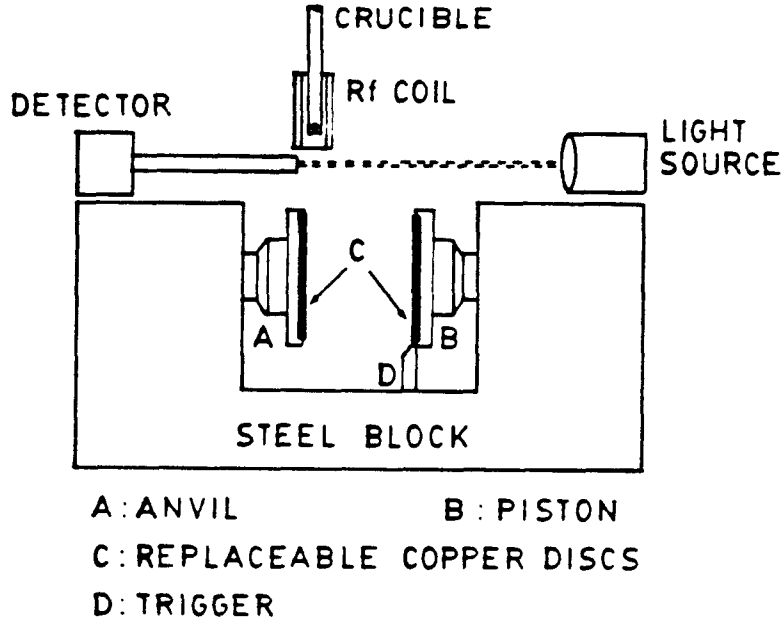

Figure 2.1 Schematic diagram of the piston and anvil rapid quenching apparatus. A metal charge is melted by RF heating in a fused silica crucible and allowed to drop vertically. When the drop interrupts the light beam, the trigger, D, allows the piston, B, to meet the anvil, A, just as the drop arrives [after Mehra, 1984].

beam on its way down. A photodetector senses the passage of the drop and triggers the pneumatically loaded piston to drive into a stationary anvil. Both piston and anvil have a copper-beryllium alloy disc on their exposed surfaces. The liquid drop is caught just as the piston and anvil meet, causing the drop to spread out and rapidly solidify into a foil 30-50 microns thick. Models of the piston and anvil quench process show that quench rates on the order of 10^5 to 10^6 K/sec are achieved [Kroeger et al., 1982].

2.2c Mechanical Alloying

For the equilibrium phase diagram study, the Al-Ru alloy ingots were mechanically alloyed for nine hours in a Spex 8000 table-model mixer mill. The mixer mill was used to produce a fine powder from the alloy ingots. The powders could then be conveniently analyzed by x-ray analysis and by differential thermal analysis. The mixer mill is illustrated in Figure 2.2 [Schwarz et al., 1985]. An alloy powder or mixture of elemental powders is placed in a canister along with six 1/2 inch diameter balls. The canister, lid and balls are made of either hardened steel or tungsten carbide. The canister is sealed with a cork ring inside the flowing argon atmosphere described in Section 2.2a. The canister is loaded into a holder, which is connected by means of a universal joint and belt to a motor. When the motor is running, the canister executes a rapid and irregular figure-eight motion, with maximum speeds on the order of 20-30 meters/sec. The powder inside the canister is intimately mixed and mechanically deformed by being trapped during collisions between the balls or between a ball and the wall.

2.3 Sample Characterization

Once a sample has been prepared, a series of tests must be performed to determine which phases are present. In this section we discuss these sample characterization techniques.

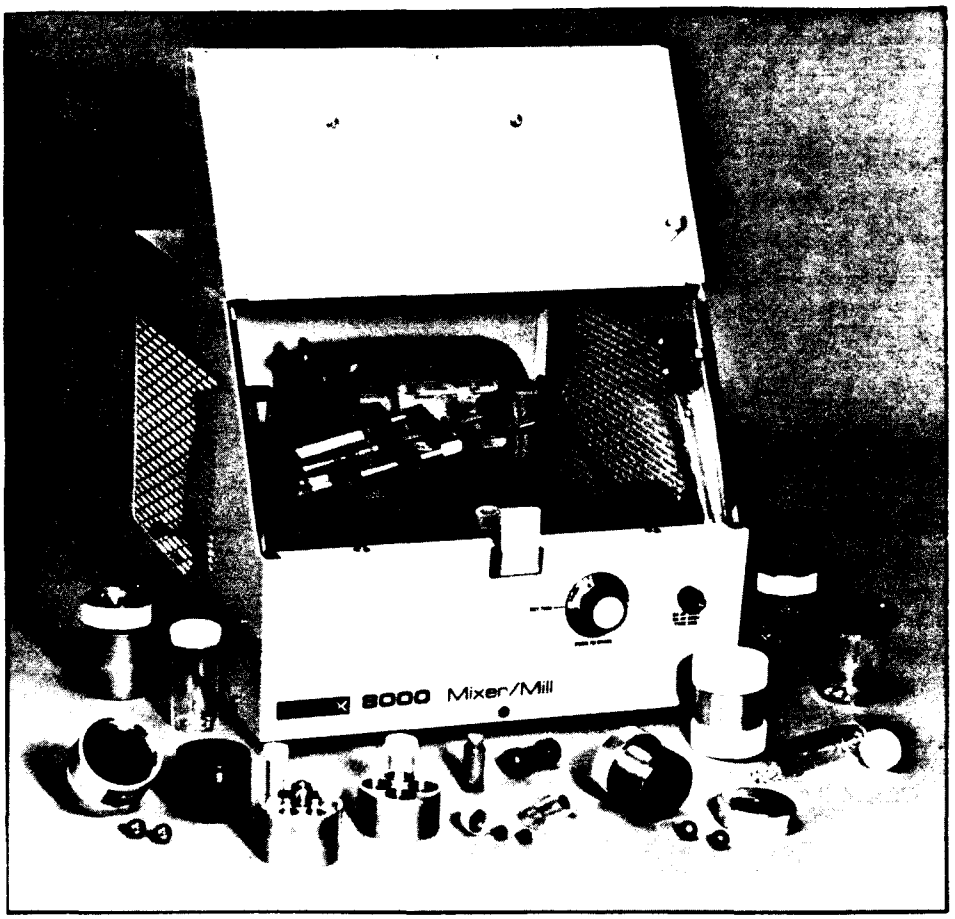

Figure 2.2 The Spex 8000 Mixer Mill used for mechanical alloying experiments. A hardened steel canister containing Al-Ru powder and six hardened steel balls is shaken in an irregular figure eight motion by means of a motor [after Spex Industries].

2.3a X-ray Diffraction

Piston and anvil quenched foils are ideally suited for analysis by means of x-ray diffraction. As shown in Figure 2.3, the flat sample is placed in the center of a focussing circle with the x-ray source and detector on the circle. X-rays undergo Bragg diffraction from parallel planes of atoms in the sample. All crystalline and quasi-crystalline materials have a unique and distinctive collection of Bragg diffraction peaks arising from their structure. Figure 2.4 shows a typical x-ray pattern of an $Al_{86}Ru_{14}$ piston and anvil quenched alloy. This sample contains the icosahedral phase (broad peaks) as well as the Al-Ru solid solution (narrow peaks).

X-ray diffraction experiments were performed on a Philips $\theta-2\theta$ diffractometer, a Debye-Scherrer camera and a Scintag Pad-V $\theta - 2\theta$ diffractometer. In all cases Ni filtered Cu K_α radiation was used.

2.3b Differential Thermal Analysis

Thermal analysis of the alloys was performed on a Perkin Elmer Differential Thermal Analyzer (DTA) for temperatures ranging up to 1400°C. The DTA was equipped with alumina sample holders and run in a computer-simulated differential scanning calorimetry mode. All runs were performed in a purified argon atmosphere flowing at a rate of 10 to 15 cm^3/min.

Thermal analysis was used to determine transition temperatures and latent heats for transitions between phases of the samples. The samples used were initially mechanically alloyed powders or mixtures of elemental powders.

2.3c Atomic Absorption Spectroscopy

Several Al-Ru ingots used in the nonequilibrium phase diagram study were analyzed by means of atomic absorption spectroscopy. This analysis provided an independent composition determination and was performed by the International

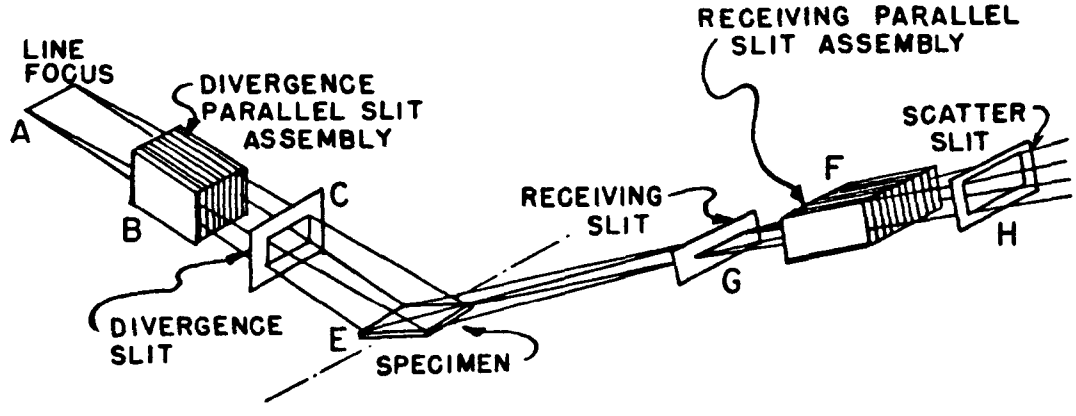

Figure 2.3 The Philips vertical goniometer used for x-ray analysis of rapidly quenched Al-Ru alloys. An x-ray tube anode line source produces an incident beam through divergence Soller slits to illuminate the specimen. The Bragg diffracted beam leaves the specimen at the angle of incidence and proceeds through a receiving Soller slit to the detector [after Philips Corporation].

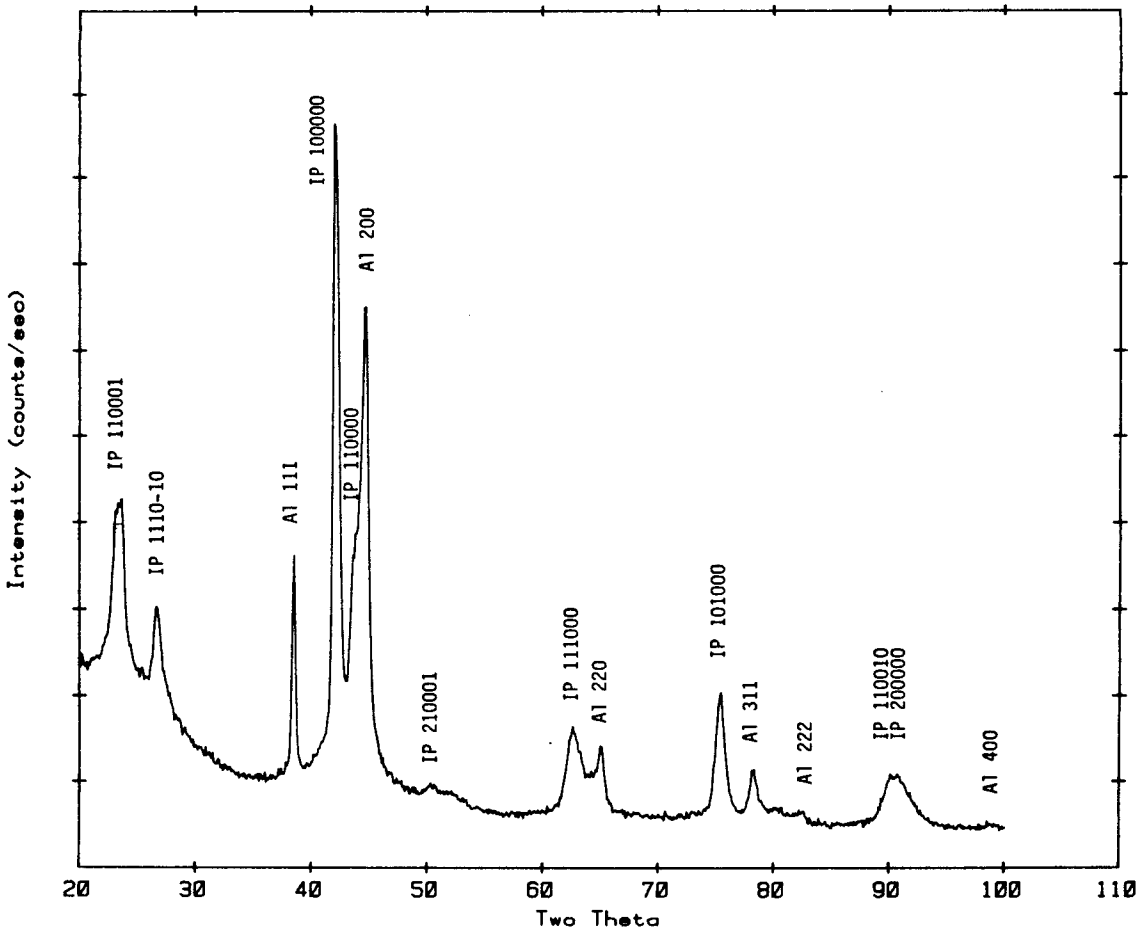

Figure 2.4 An x-ray diffraction pattern of a piston and anvil quenched $Al_{86}Ru_{14}$ alloy. The diffraction peaks can be indexed to an Al-Ru solid solution (sharp peaks) and icosahedral Al-Ru (broad peaks). The icosahedral phase diffraction peaks are labelled with the indexing convention of Bancel et al. [Bancel et al., 1985].

Technology Corporation. The composition determinations made by atomic absorption spectroscopy, energy dispersive x-ray analysis (Section 2.3d) and in alloy preparation are all in agreement to within 2 at% Ru.

2.3d Electron Microscopy

Samples to be studied by transmission electron microscopy (TEM) must first be thinned down to electron transparency (<1000Å). Two techniques were employed for doing this. Most of the sample thickness reduction is done by electrochemical polishing on a Fishione jet electropolisher. Samples were cut into 3mm diameter discs and thinned to electron transparency with a solution of methanol and perchloric acid at -40°C. The samples were then ion-milled at a shallow angle to remove organic deposits and oxides left over from the chemical thinning process. A VCR dual-gun argon ion-mill was used for this purpose.

The TEM work was performed on a variety of instruments, including a Siemens Elmiskop I operated at 100kV, a Philips 400 scanning transmission electron microscope (STEM) operated at 120 kV, a JEOL 200CX STEM operated at 200 kV with a Kevex x-ray analysis unit as well as a Philips EM430 STEM operated at 300 kV and equipped with an EDAX energy dispersive x-ray analysis unit. Through the manufacturers' software, the intensities of the Al K peaks and Ru L peaks were determined and converted into chemical concentrations by a standardless thin-film analysis technique. The thin-film analysis assumes that the electron beam passes through the sample with only a small amount of spreading, so that the x-ray absorption and secondary fluorescence can be ignored. Quantitative analysis was performed only on areas of the sample where the thin-film condition was satisfied. Energy dispersive x-ray analysis was performed at selected spots as well as on a line of spots through an icosahedral particle and into its neighboring matrix.

For the equilibrium phase diagram study, scanning electron microscopy (SEM) was performed with a Cam-Scan Series 4 SEM. Standardless energy dispersive x-ray

analysis was performed on as-cast alloy ingots, using a Kevex x-ray analysis unit through a 20 μm thick Be window.

Chapter 3 Experimental Results and Discussion

The Al-Ru icosahedral phase-forming system has been chosen to study the conditions under which the icosahedral phase forms from the melt. To better understand the results of the rapid quenching experiments, it proved necessary to determine the equilibrium Al-Ru phase diagram in the region where the rapid quenching experiments took place. In Section 3.1 we present the results of this determination. In Section 3.2 the rapid-quenching nonequilibrium phase diagram is presented. This is followed by a discussion of the mobility of ruthenium during the rapid quench, leading to the conclusion that ruthenium segregation to the growing icosahedral particles takes place through the liquid phase.

3.1 The Equilibrium Al-Ru Phase Diagram

Figure 3.1 presents the recently determined equilibrium $Al_{1-x}Ru_x$ phase diagram for $x < 25$ at% [Anlage et al., 1987]. This region of the phase diagram is where the Al-Mn icosahedral phase is found to form [Shechtman et al., 1984] and where the Al-Ru icosahedral phase is also expected to form. There are three compounds in this region. The Al-Ru face-centered cubic solid solution extends out to approximately 0.03 at% Ru [Varich and Lyukevich, 1973]. The Al_6Ru compound is orthorhombic with space group Cmcm [Edshammar, 1968]. The morphology of the Al_6Ru compound is shown in a scanning electron micrograph (SEM) image (Figure 3.2) of an as-cast $Al_{80}Ru_{20}$ ingot. The $Al_{13}Ru_4$ compound is monoclinic with space group C2/m [Edshammar, 1965]. Figure 3.3 is an SEM micrograph showing $Al_{13}Ru_4$ crystals in the same as-cast $Al_{80}Ru_{20}$ ingot.

From Figure 3.1 we see that the Al-Ru solid solution eutectic is at 652°C, approximately 8°C below the melting temperature of elemental Al. The Al_6Ru compound melts peritectically at 723°C into $Al_{13}Ru_4$ and an aluminum-rich liquid. In the course of the thermal analysis measurements it was observed that

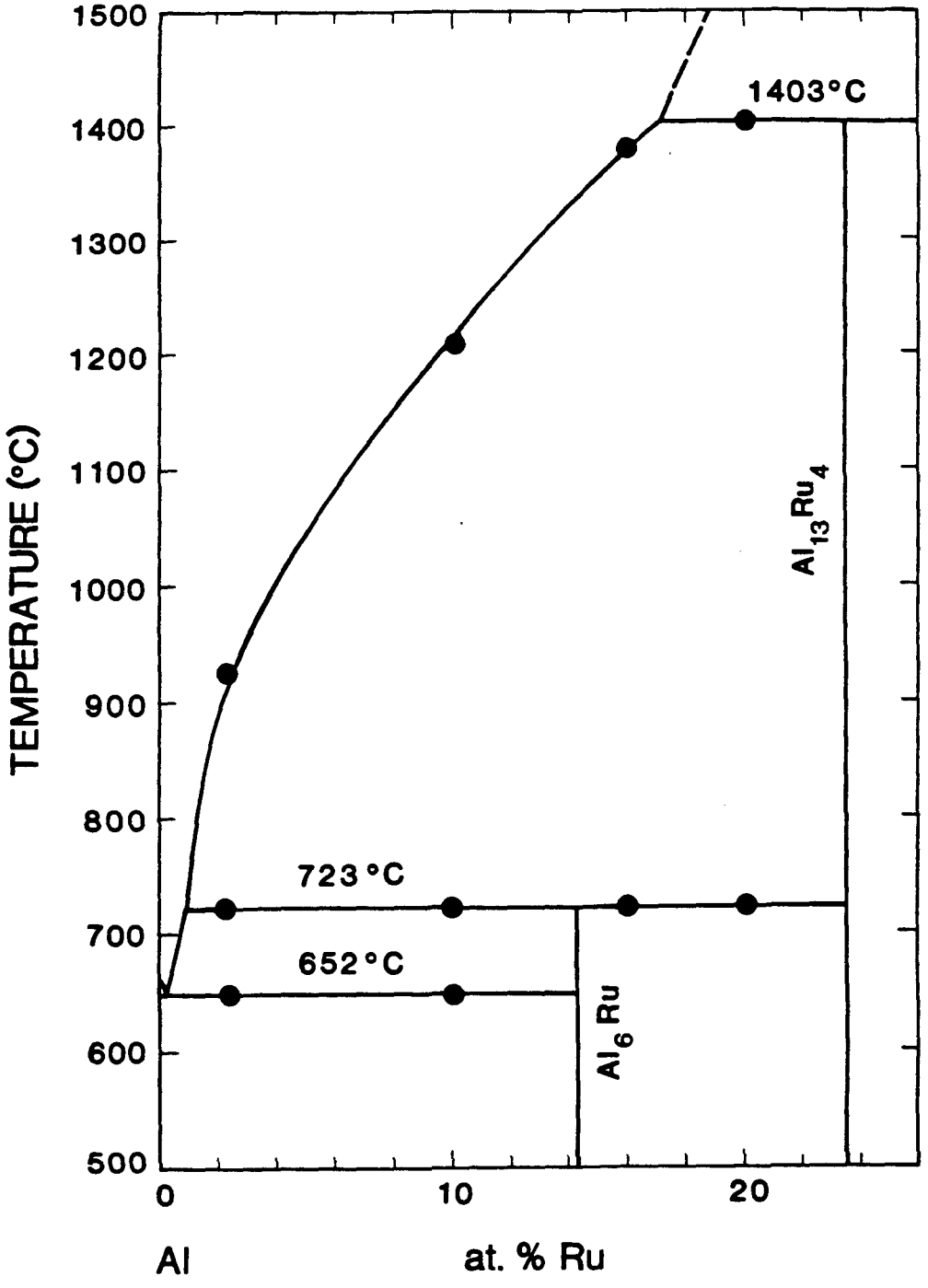

Figure 3.1 Equilibrium phase diagram for the Al-rich end of the Al-Ru system. Solid symbols represent measured values.

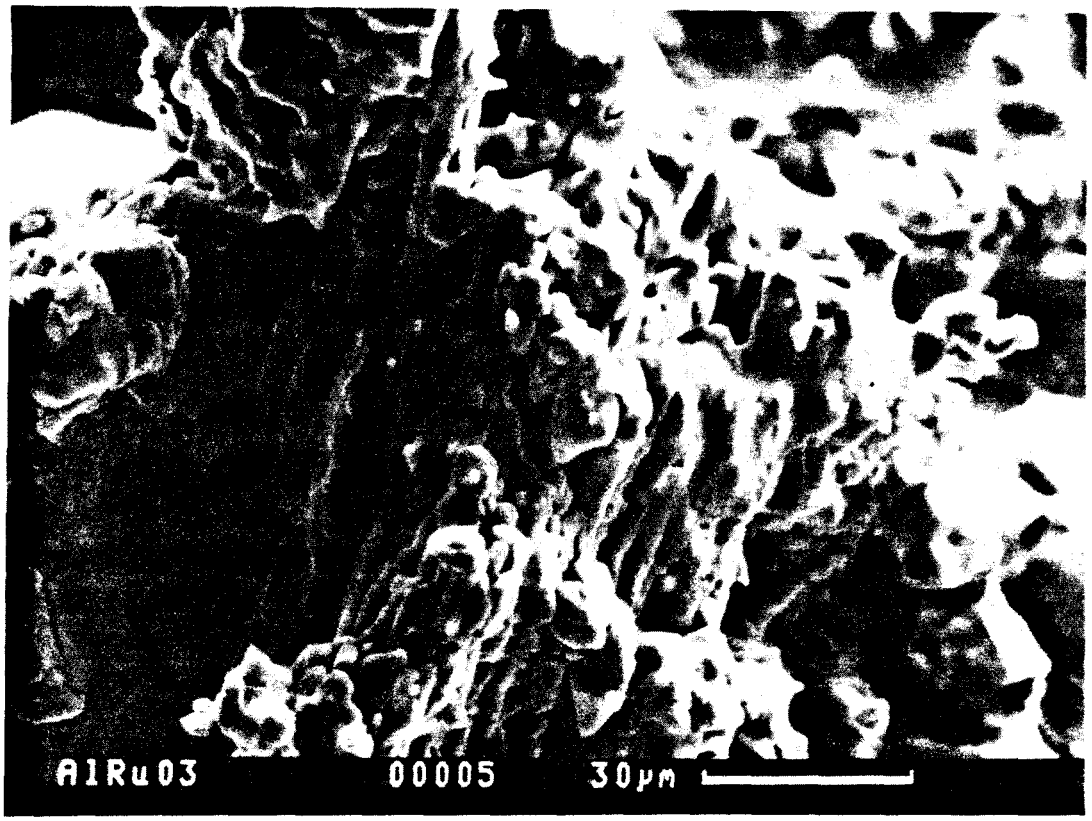

Figure 3.2 A scanning electron micrograph showing Al_6Ru crystals in the as-cast $Al_{80}Ru_{20}$ alloy.

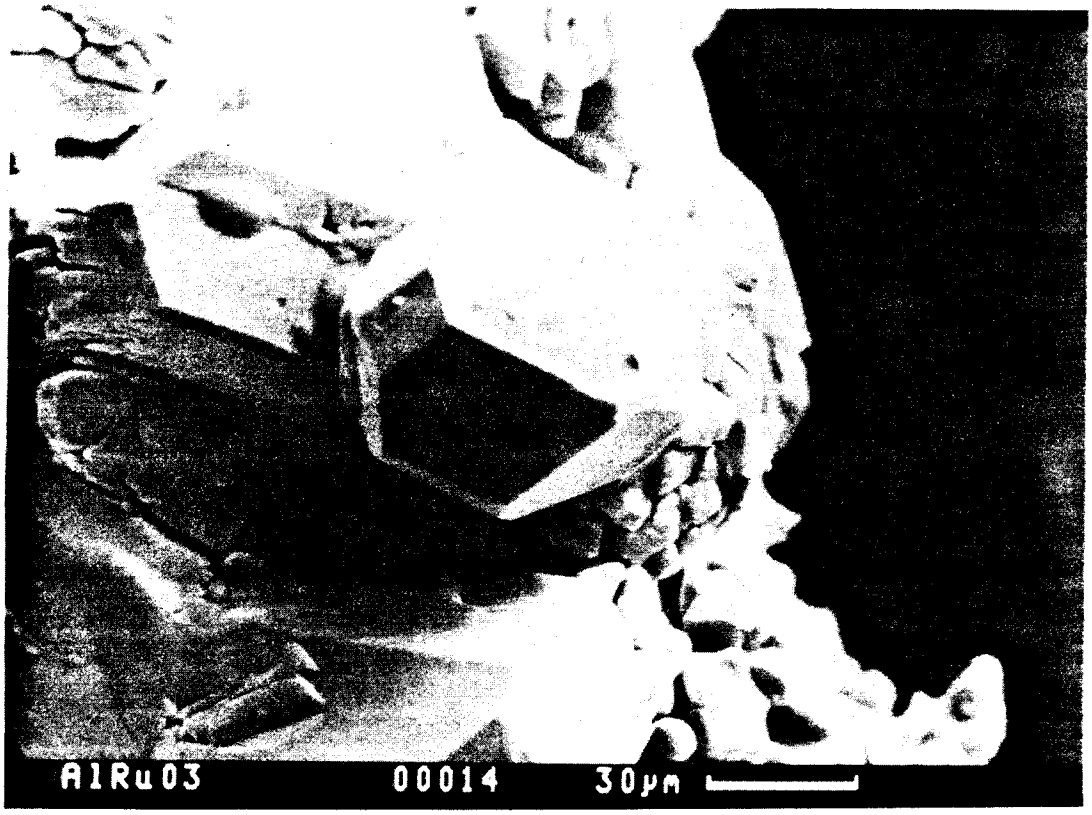

Figure 3.3 A scanning electron micrograph showing $Al_{13}Ru_4$ (faceted crystal in center) in the as-cast $Al_{80}Ru_{20}$ alloy.

growth of the Al_6Ru phase was easily suppressed upon quenching from the two-phase liquid+$Al_{13}Ru_4$ region above 723°C. Al_6Ru must grow peritectically through a reaction between the relatively stable $Al_{13}Ru_4$ intermetallic and an Al-rich liquid at 723°C. This growth is nucleated heterogeneously at the surface of $Al_{13}Ru_4$ crystals, but because of the low reaction temperature does not proceed to completion on laboratory time scales. This is illustrated in Figure 3.4, which shows that a thin boundary layer of Al_6Ru has formed between $Al_{13}Ru_4$ and the (subsequently solidified) Al-Ru solid solution, despite a relatively slow quench rate of 1 K/min. The growth of Al_6Ru is limited by diffusion of Ru out of $Al_{13}Ru_4$ and must also take place at low temperatures. Hence, growth of this phase will be relatively easy to avoid during a rapid quench of the liquid to room temperature.

The $Al_{13}Ru_4$ compound melts peritectically at 1403°C into an Al-Ru liquid and an unknown Al-Ru compound. These high-temperature product phases could not be investigated carefully because they exist at the extreme limits of the thermal analysis equipment.

From work on the Al-Mn icosahedral phase [Krishnan et al., 1986], it is known that the Al-Ru icosahedral phase is expected to have a composition of about $Al_{80}Ru_{20}$. Because the growth of Al_6Ru is largely suppressed at moderate quench rates, there are only two intermetallic compounds competing for formation with the metastable icosahedral phase during a rapid quench of the liquid. The Al-Ru icosahedral phase should then form over a relatively wide (2 to 23 at% Ru) composition range after a rapid quench.

3.2 The Nonequilibrium Al-Ru Phase Diagram

Rapid quenching experiments have been performed on a series of $Al_{1-x}Ru_x$ alloys for x=2.5, 5, 7.5, 10, 12.5, 14, 15 and 20 at% Ru. The results of all of these experiments can be summarized on a single nonequilibrium phase diagram, shown in Figure 3.5. Also shown, in dotted lines, is the equilibrium phase diagram presented

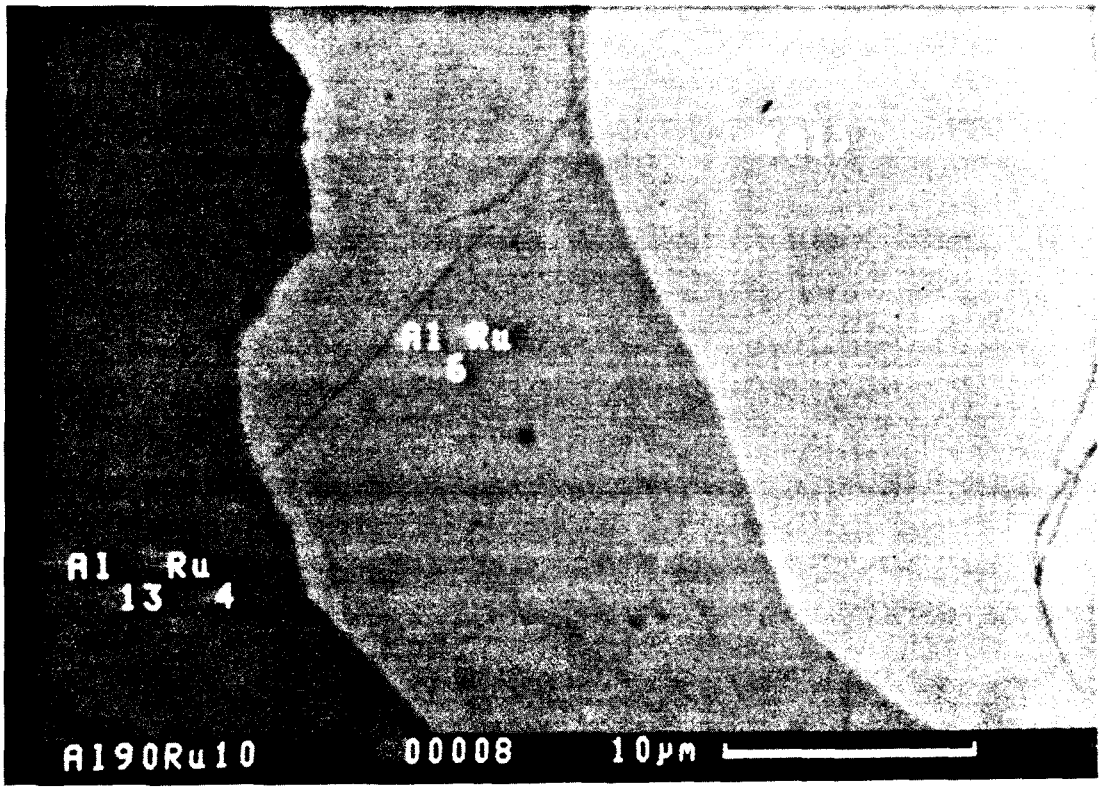

Figure 3.4 A scanning electron micrograph showing the structure of an $Al_{90}Ru_{10}$ ingot after cooling in the calorimeter at the rate of 1 K/min. Peritectic formation of Al_6Ru is evident at the boundary between $Al_{13}Ru_4$ and the Al-rich matrix.

in Section 3.1. All of the compositions shown in this diagram have been measured, but most of the temperatures shown are schematic. For instance, the liquidus curves shown are depressed by several hundred degrees below the equilibrium liquidus to represent the undercooling expected to occur during a rapid quench of the liquid. As expected, the growth of Al_6Ru was so strongly suppressed by the quench that none was observed (i.e., below the detection limit of x-ray analysis, <1 %) in any of the rapidly quenched alloys.

The nonequilibrium phase diagram shows three phases; an Al-Ru solid solution, which extends to 2.4 at% Ru (our measured value is somewhat less than the 3.2 at% Ru determined from x-ray analysis by Varich and Lyukevich [Varich and Lyukevich, 1973]), the icosahedral phase, and the compound $Al_{13}Ru_4$ [Edshammar, 1965]. The composition of the icosahedral phase was determined to be approximately 19 at% Ru from x-ray chemical analysis of the grains in rapidly solidified $Al_{1-x}Ru_x$ for $0.025 \leq x \leq 0.10$. We have represented the icosahedral phase as a compound with a wide phase field, since it is known to be somewhat tolerant of chemical disorder [Schaefer, 1986]. Energy dispersive x-ray line scans through the icosahedral particles showed some enhancement of Ru concentration near the centers of the particles. For this reason, the icosahedral phase region in Figure 3.5 widens slowly at lower temperatures. However, the difference in composition between the edge and center of the particles was 2.5 at% Ru, which is only slightly greater than the resolution of these measurements.

Changing the quench rate of the liquid will change the features of the non-equilibrium phase diagram in Figure 3.5. Decreasing the quench rate has the effect of replacing the icosahedral phase with the decagonal phase [Bendersky et al., 1985a]. The decagonal phase has a tenfold symmetric quasi-periodic structure in two dimensions and is periodic in the third [Bendersky, 1985b]. A further decrease in the quench rate results in the formation of crystals in accordance with the equi-

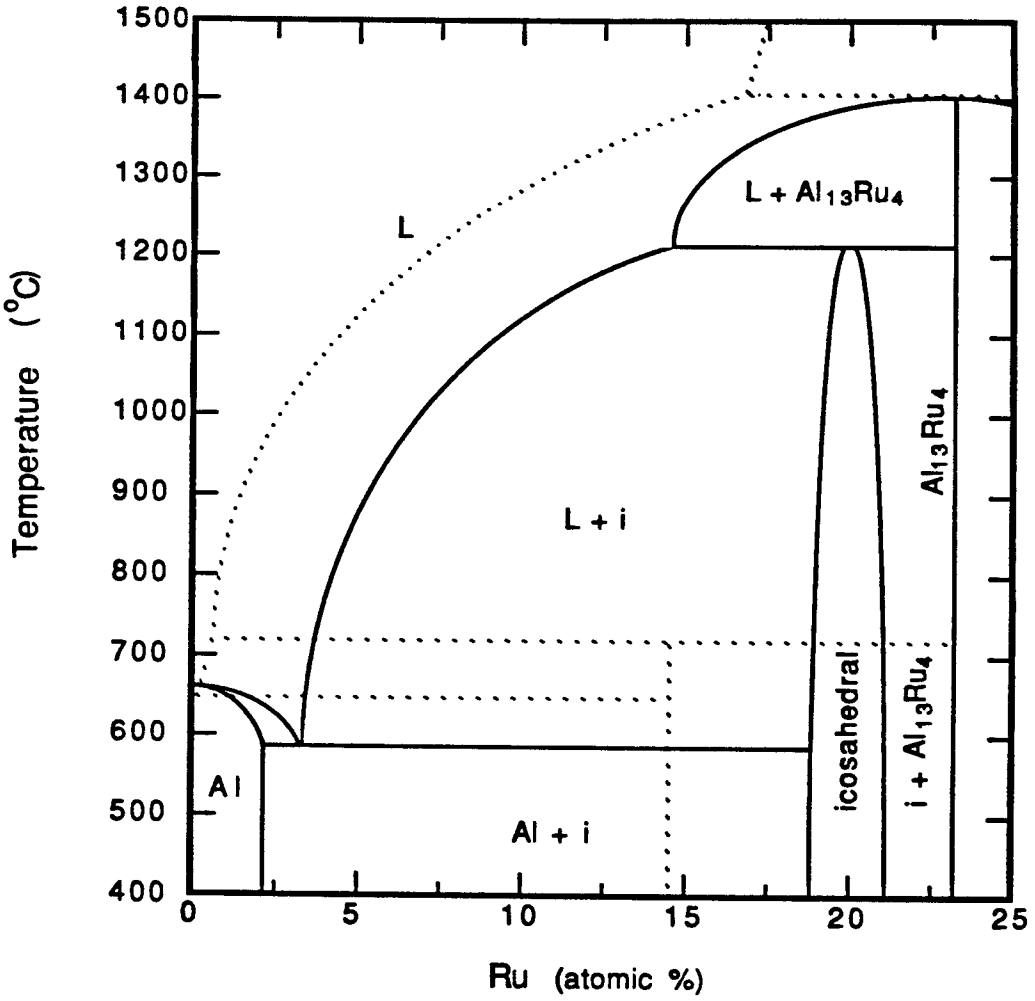

Figure 3.5 Schematic piston and anvil non-equilibrium liquid quenching phase diagram for the $Al_{1-x}Ru_x$ system for x < 25 at% Ru. Dotted lines indicate the equilibrium phase structure as determined by Anlage et al. [Anlage et al., 1987]. Vertical dotted lines show the Al_6Ru and $Al_{13}Ru_4$ phases. A dotted region in the upper right corner shows equilibrium between another Al-Ru compound and the liquid phase.

librium phase diagram, Figure 3.1. An increase in the quench rate results in the formation of a metallic glass [Bendersky and Ridder, 1986]. In fact, Bendersky and Ridder use their experimental results to arrive at the following conclusions: (i) The icosahedral phase forms by homogeneous nucleation in the liquid during a rapid quench, (ii) The possible topological similarities between the liquid and icosahedral phase can explain the low nucleation resistance of the icosahedral phase, and (iii) An Al-Mn glass may not be a configurationally frozen liquid but instead, a nano-icosahedral phase.

In Part II of this thesis we arrive at the same conclusion as point (i). In Part III we shall discuss a model of a predominantly icosahedral material that uses point (ii) as its starting hypothesis (i.e., that there is a similarity in the short-range structure of the liquid and icosahedral phase). Conclusion (iii) is the concept that originally motivated this research (i.e., that a theory of the structure of metallic glasses can be based on a frustrated packing of noncrystallographic structures), but will not be discussed here.

Because many of the rapidly quenched Al-Ru samples contained three phases, we cannot represent the results of our experiments on a single equilibrium or metastable equilibrium [Perepezko and Boettinger, 1983] binary phase diagram. One must apply a few simple rules to understand and use this nonequilibrium phase diagram. First, the diagram can be used only to determine the solid end products that would result from a rapid quench (by the piston and anvil method) of the liquid down to room temperature. Secondly, any solid phase that forms in the course of the quench will be preserved at lower temperatures. This means that solid phases will accumulate during the quench, since they do not have time to decompose into their "equilibrium" products at lower temperatures (unless they transform polymorphically).

As a simple application of these rules, consider the results of a rapid quenching

experiment performed on an $Al_{80}Ru_{20}$ liquid. Upon quenching the liquid from high temperature, the first solid phase to form is $Al_{13}Ru_4$. This phase forms during the excursion through the two-phase liquid+$Al_{13}Ru_4$ region. Upon further cooling, the Al-Ru icosahedral phase will form exclusively from the liquid. The result of the quench is then a two-phase mixture of $Al_{13}Ru_4$ and Al-Ru icosahedral phase. Close examination of this diagram shows that it is impossible to obtain a single phase icosahedral Al-Ru sample through rapid quenching by the piston and anvil technique.

The horizontal tie line representing the peritectic formation temperature of icosahedral Al-Ru is estimated from the nonequilibrium melting measurements of Knapp and Follstaedt [Knapp and Follstaedt, 1987a]. In their experiments, thin films of single phase icosahedral Al-Ru are produced on a sapphire substrate [Follstaedt and Knapp, 1987a; 1987b] and then rapidly annealed by a scanning electron beam. The films are annealed and quenched at rates of $\approx 5 \times 10^6$ K/sec and 2×10^6 K/sec, respectively, so that no solid state transformations are possible [Knapp and Follstaedt, 1987a]. By carefully controlling the peak temperature achieved in the films and observing the resulting microstructure, Knapp and Follstaedt have determined that the temperature at which the free energy of the Al-Ru liquid equals the free energy of the icosahedral Al-Ru solid is 1230±40°C [Knapp and Follstaedt, 1987b]. This temperature, sometimes referred to as T_0, represents the temperature at which the solid icosahedral Al-Ru undergoes polymorphic melting. We have used this temperature as an upper bound of the icosahedral Al-Ru peritectic point.

The fact that T_0 represents an upper bound on the peritectic formation temperature of icosahedral Al-Ru can be seen from Figure 3.6. At $T=T_0$, the system is a two-phase mixture of $Al_{13}Ru_4$ and Al-rich liquid, with compositions and concentrations given by the common tangent shown. The $Al_{81}Ru_{19}$ icosahedral phase has a Gibbs free energy well above the common tangent. At $T = T_p < T_0$, the

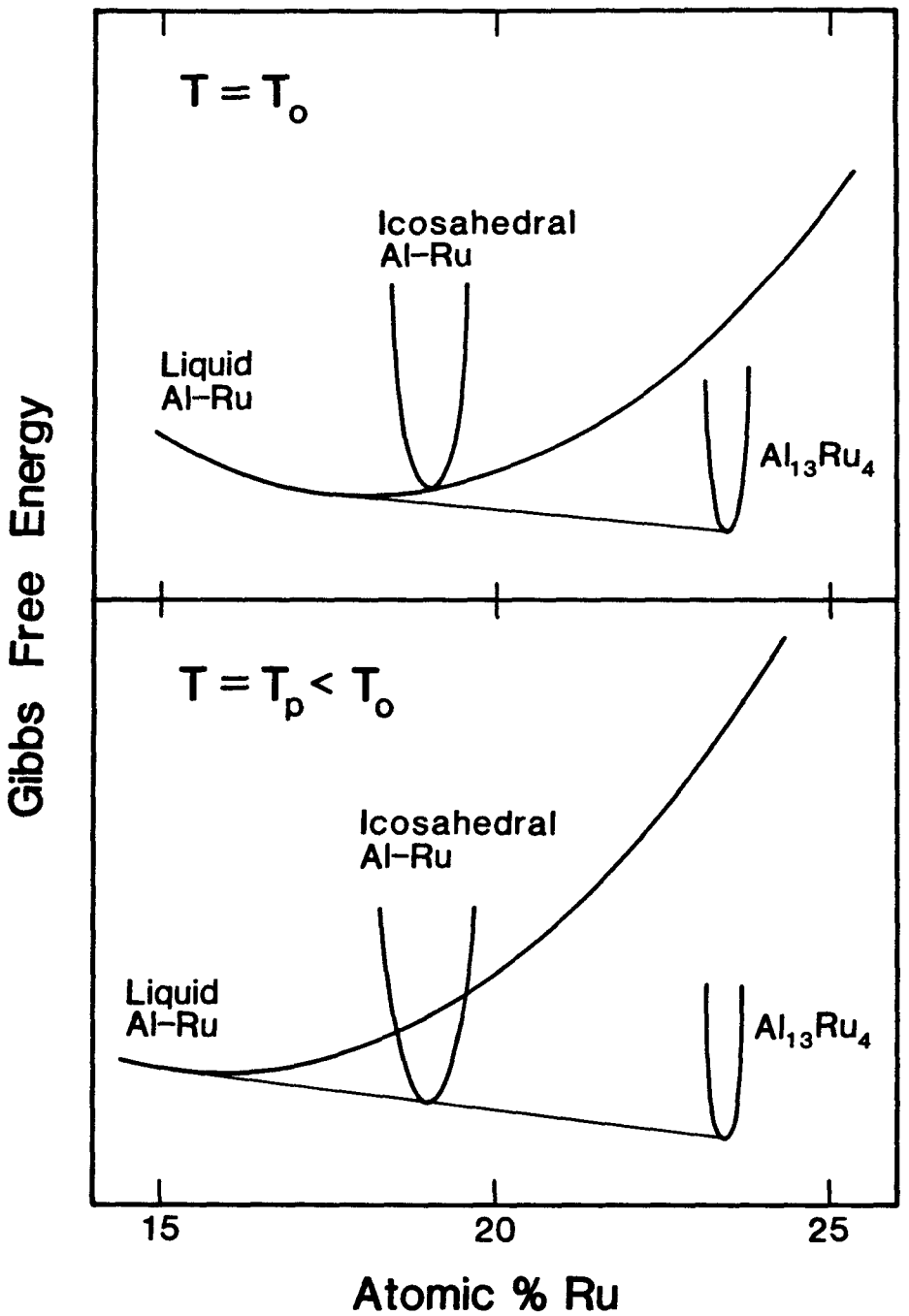

Figure 3.6 Schematic Gibbs free energy versus Ru composition for liquid Al-Ru, icosahedral Al-Ru and $Al_{13}Ru_4$. The icosahedral phase begins to form peritectically at $T = T_p$.

$Al_{81}Ru_{19}$ free energy first breaks through the common tangent and it begins to form peritectically.

3.3 Ruthenium Segregation to the Icosahedral Grains

By examining the microstructure of rapidly quenched Al-Ru alloys, we can deduce an interesting fact about how the icosahedral phase forms from the liquid.

3.3a Sample Morphology

The icosahedral phase was found by TEM or x-ray analysis in all of the rapidly solidified alloys studied. Figures 3.7 and 3.8 show the general morphology of two of these rapidly solidified alloys. Analytical STEM analysis of the icosahedral phase particles showed that they contain concentrations of ruthenium well above the nominal composition of the alloy, and the surrounding matrix is depleted in ruthenium.

The particles in rapidly quenched $Al_{90}Ru_{10}$ (Figure 3.7), $Al_{92.5}Ru_{7.5}$ and $Al_{95}Ru_5$, show the characteristic rosette structure seen in most other Al-transition metal icosahedral phase-forming systems. On the other hand, particles of the icosahedral phase in $Al_{97.5}Ru_{2.5}$ (Figure 3.8) do not form rosettes, but have a simple equi-axed shape. This change in morphology is explained by the eutectic feature in Figure 3.5. The rapidly quenched alloys $Al_{1-x}Ru_x$ with $3 < x < 14$ at% Ru will form the icosahedral phase directly from the Al-rich liquid, and subsequently form an Al-Ru solid solution at a lower temperature. For the $Al_{97.5}Ru_{2.5}$ alloy, however, the Al-Ru solid solution forms first. The Al-Ru icosahedral phase then forms at a lower temperature in the "puddles" of excluded Ru in the frozen Al matrix. This lower formation temperature and the constrained geometry accounts for the difference in shape of the icosahedral particles.

X-ray diffractometry (XRD) of rapidly solidified $Al_{86}Ru_{14}$ showed the presence of both the Al-Ru icosahedral phase and the Al-Ru FCC solid solution. An XRD pattern of rapidly quenched $Al_{85}Ru_{15}$ showed that Al, the Al-Ru icosahedral phase

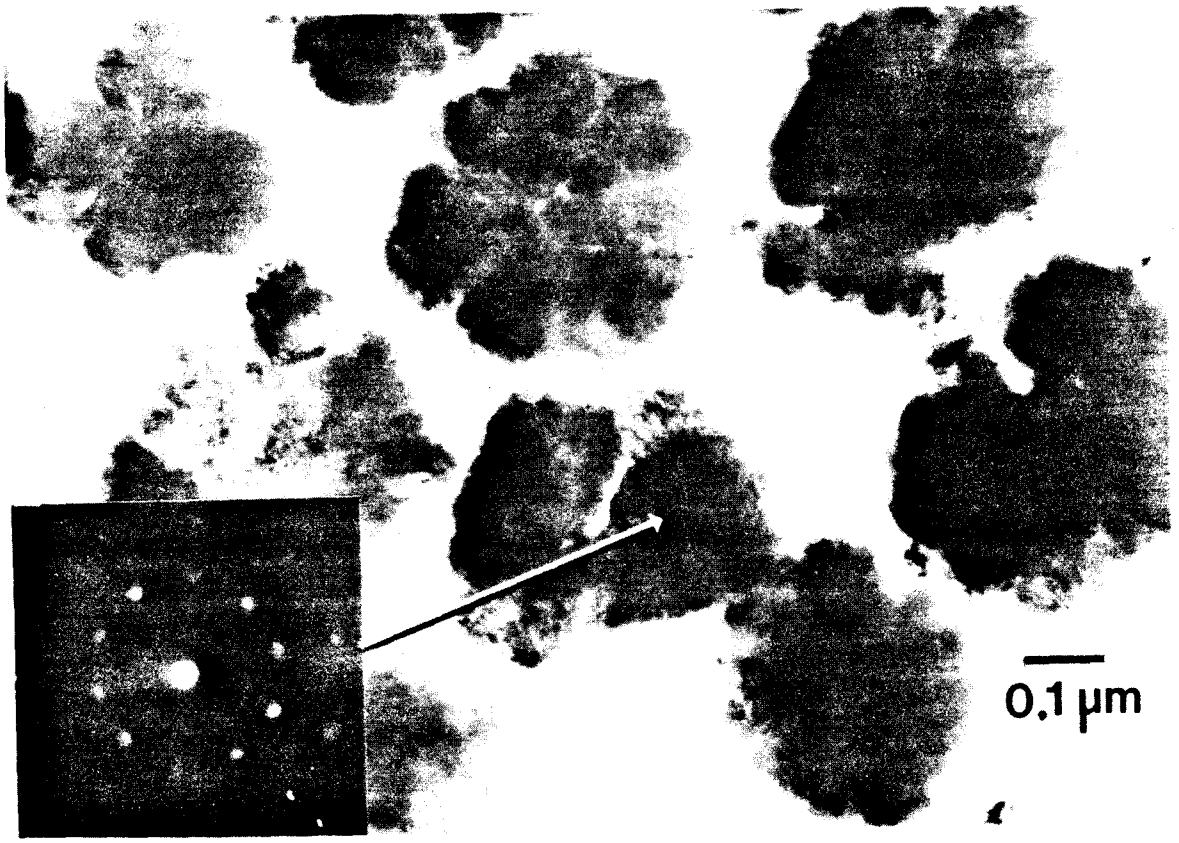

Figure 3.7 Bright field image from piston and anvil quenched $Al_{90}Ru_{10}$ showing the rosette shaped icosahedral particles surrounded by aluminum matrix. An arrow shows the approximate location where the fivefold diffraction pattern (inset) was obtained.

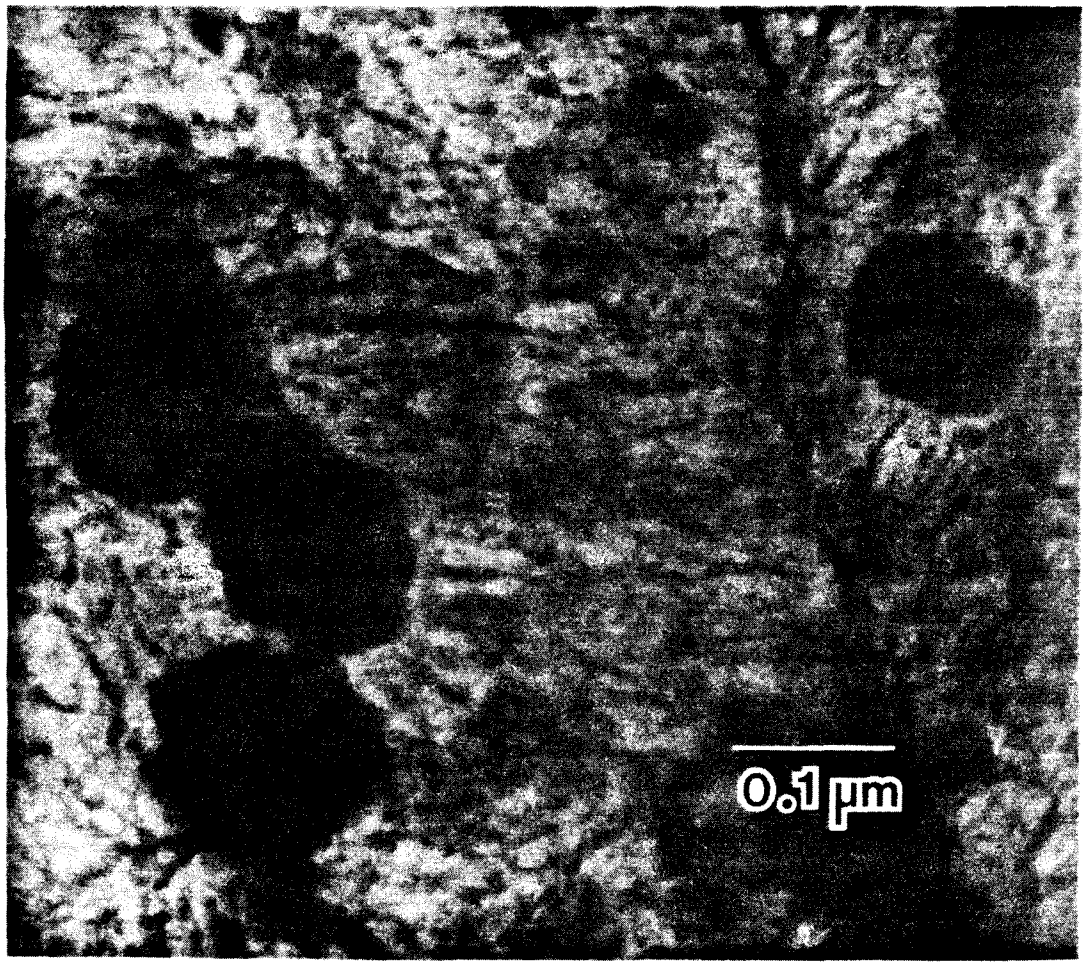

Figure 3.8 Bright field image from piston and anvil quenched $Al_{97.5}Ru_{2.5}$ showing the equi-axed icosahedral particles surrounded by an aluminum matrix.

and $Al_{13}Ru_4$ were all present in substantial amounts. Finally, XRD analysis of rapidly quenched $Al_{80}Ru_{20}$ revealed that the alloy is mostly $Al_{13}Ru_4$ with a smaller amount of icosahedral material. In all of the alloys studied, we have never found an example of single phase icosahedral phase material being made by liquid quenching.

3.3b Ruthenium Segregation

The strong segregation of Ru to particles of the icosahedral phase implies a large diffusivity for Ru in the melt. If we define a diffusion length r_d such that all Ru in excess of the matrix solubility diffuses over this length to a particle of the icosahedral phase, we have the relationship

$$r_d = r_p \left(\frac{x_i - x_0}{x - x_0} \right)^{1/3},$$

where r_p is the radius of the (spherical) icosahedral particle, x_i is its concentration of Ru, x is the Ru concentration in the bulk alloy, and x_0 is the solubility of Ru in the Al matrix. Through x-ray chemical analysis we have found the concentration x_i=0.19 for all alloys with Ru concentrations, x, between 0.025 and 0.10. We have measured r_p for the largest particles found in TEM micrographs of each alloy. (The size distribution of icosahedral particles is rather sharp and is skewed towards small particle sizes. For diffusion analysis, we chose to consider the largest particles because it is most likely that they formed early and were least affected by the diffusion fields of neighboring particles.) We find that the volume of the largest icosahedral phase particles present increases linearly with Ru concentration x. A value of x_0=0.024 was determined as the concentration at which the volume of icosahedral phase particles extrapolates to zero (i.e., the concentration at which only the Al-Ru solid solution is present). From the formula above, we calculate $r_d \simeq 0.5$ μm for all alloy compositions between x = 0.025 and x = 0.10. Assuming a diffusion time of 10^{-4} seconds during the rapid cooling [Kroeger et al., 1982],

we deduce a diffusivity for Ru on the order of $10^{-5}cm^2/sec$. This high diffusivity indicates that the icosahedral phase forms directly from the liquid.

3.4 Conclusions

The high diffusivity of Ru during icosahedral phase formation in the rapid quench implies that the Al-Ru icosahedral phase grows directly from the melt. From Figure 3.1 one sees that the Al-Ru icosahedral phase nucleates first from the melt for alloys $Al_{1-x}Ru_x$, with $3 \leq x \leq 14$ at% Ru. With the absence of pre-existing nuclei, this means that the icosahedral phase nucleates homogeneously from the melt.

In Chapter 1 it was shown that many metallic systems display noncrystallographic, and in particular, icosahedral, clustering on atomic length scales. It may be that icosahedral clustering occurs in supercooled liquid Al-Ru and the icosahedral phase nucleates from the larger fluctuating clusters. Is this kind of short-range order a necessary prerequisite for the formation of an icosahedral phase? We shall answer this question in Section III by examining the thermodynamics of a predominantly icosahedral material, i.e., one that is endowed with short-range icosahedral order.

III. A Theory of Icosahedral Phase Formation

Chapter 4 The Predominantly Icosahedral Material

4.1 Icosahedral Short-Range Order and Icosahedral Phase Formation

In Chapter 1 it was mentioned that extensive icosahedral clustering has been observed on the atomic length scale in large unit cell intermetallic crystals. Icosahedral clusters are also believed to exist in supercooled liquid metals and rapidly quenched metallic glasses. Since the icosahedral phase is normally formed upon rapid quenching of the liquid, it may nucleate on the icosahedral clusters present in the supercooled liquid. If this is the case, then icosahedral clustering is a necessary prerequisite for formation of the icosahedral phase.

In Part III, we shall discuss a model material which is endowed with only short-range icosahedral order, in analogy with a supercooled liquid metal. We shall study the behavior of this model material as a function of temperature and show that there exists a high-temperature, disordered phase as well as a low-temperature phase with enhanced short-range icosahedral order. The behavior of this model is then compared to the measurements presented in Part II, and numerical values for several key quantities will be calculated.

The results of Part III are summarized in a paper delivered to the International Workshop on Quasi-crystals, held in Beijing, China, during September, 1987 [Anlage, 1987]. In Appendix I, we give a brief review of the curved space description of amorphous materials. Our concept of a predominantly icosahedral material is based on the curved space description of an icosahedral metallic glass.

4.2 The Physical Picture

The model of a predominantly icosahedral material (PIM) consists of two components. These are the order parameters which describe the two kinds of ordering present in an icosahedral material.

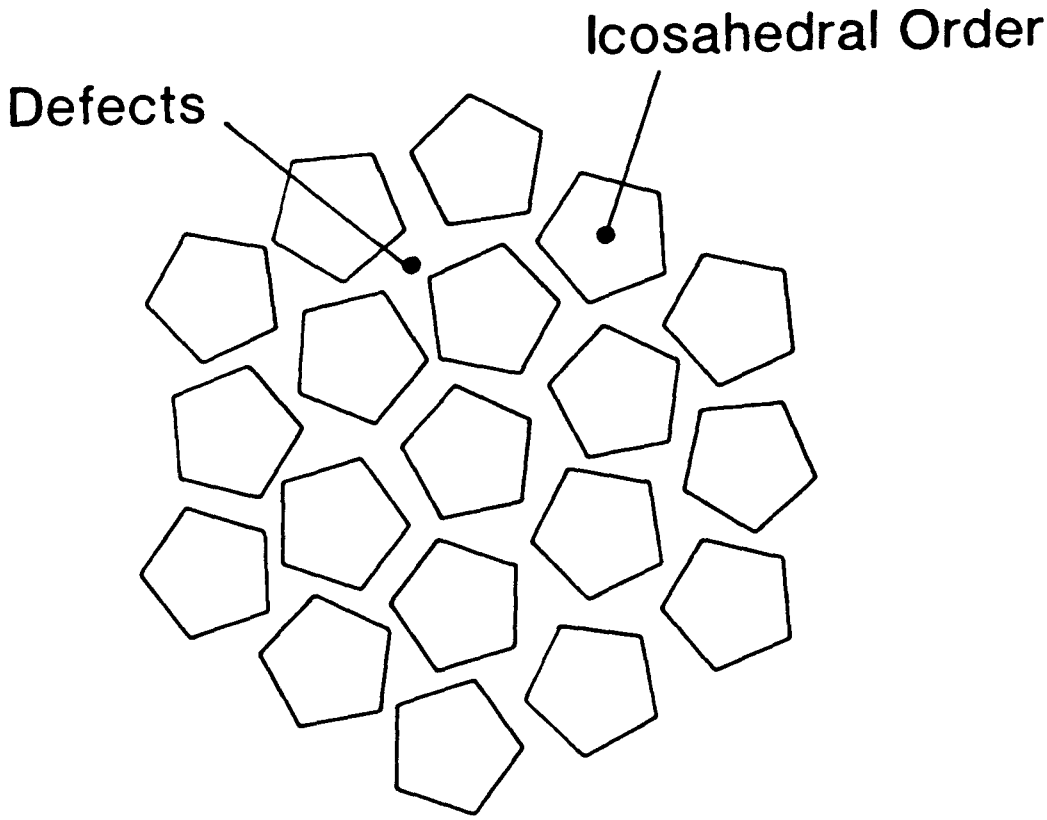

Figure 4.1 Schematic physical picture of the predominantly icosahedral material. Regions of high local icosahedral order are separated by linear defect structures.

To help visualize the theory, a schematic diagram of a PIM is shown in Figure 4.1. The PIM is characterized by small regions in which the atoms cluster into units having short-range icosahedral symmetry. These regions need not be thirteen-atom icosahedral clusters; several shells of atoms with icosahedral symmetry are also possible. Such clusters are commonly found in alloy systems with two or more atoms of different sizes. We shall define an icosahedral order parameter as having a large value in the vicinity of these icosahedral clusters. Since the icosahedral units cannot pack together to fill space, there must be some regions between them where there is little or no icosahedral order. In Section 4.4 we shall see that these regions are, in fact, linear features and will be called disclination lines, since they represent a rotational anomaly about the line. Thus a PIM can be succinctly described as regions of local icosahedral order broken up by defect line structures.

Unlike melting, where grain boundaries, interfaces and surfaces catalyze the phase transition, the freezing of a predominantly icosahedral material can be profitably modelled as a defect-mediated phase transition. Using the icosahedral order parameter and its defects, we can construct a theory for the thermodynamics of a PIM in analogy with the Ginzburg-Landau (GL) theory of superconductivity. In the GL theory, one expands the energy of the system near the transition temperature in powers of a "small" order parameter, and includes terms for the energy associated with any external fields that may be present. The Ginzburg-Landau theory of PIM exhibits a first order phase transition between a high-temperature disordered phase and a low-temperature ordered state. We shall study this transition and the two phases which it separates.

4.3 Local Icosahedral Order Parameter

A local icosahedral bond orientational order parameter has been developed by Steinhardt and Nelson. The first step is to identify the bonds (with midpoint $\vec{r}$) between a given atom and all of its neighbors. A simple set of order parameters can

be defined as the spherical harmonics $Y_{l,m}(\vec{r})$ of each bond with respect to a fixed coordinate system [Steinhardt et al., 1981]. When these quantities are averaged over all the bonds in an isotropic liquid, one expects all of the $\langle Y_{l,m} \rangle$ to vanish except for $Y_{0,0}$. For a system with cubic point group symmetry, one finds non-zero values for $\langle Y_{4,m} \rangle$, $\langle Y_{6,m} \rangle$, $\langle Y_{8,m} \rangle$, etc. [Nelson and Toner, 1981]. In the thirteen-atom icosahedral cluster, one finds the first non-zero order parameters with $Y_{6,m}$. A somewhat more sophisticated local orientational order parameter, which takes into account both orientational and translational order, was later developed by Nelson and Widom, using the curved space description of amorphous materials [Nelson and Widom, 1984]. As discussed in Section 1.4, five perfect tetrahedra wrapped around a common edge will leave a deficit angle of about 7° (see Figure 1.3). If space can be curved in such a way as to close up this deficit angle, then a tetrahedral tesselation of space may then be possible. Nelson used such a tesselation, originally proposed by Coxeter [Coxeter, 1973], known as polytope $\{3,3,5\}$. The Schläfli symbol [Coxeter, 1973] for a tetrahedron is $\{3,3\}$, denoting an object with three equilateral triangles that meet at a single point (in 3-dimensions). Polytope $\{3,3,5\}$ is a regular object with five perfect tetrahedra meeting along a common edge (in 4-dimensions).

Atoms can be assigned to the 120 vertices of polytope $\{3,3,5\}$ to produce a tetrahedral tesselation of curved 3-dimensional space. Figure 4.2 shows an "exploded view" of polytope $\{3,3,5\}$, made by taking 3-dimensional cross sections at different values of the fourth coordinate. This ideal tesselation consists of a central atom surrounded by icosahedral, dodecahedral, larger icosahedral and icosidodecahedral shells. The environment of each vertex of polytope $\{3,3,5\}$ is equivalent, and this local environment will represent what we expect to find in an ideal icosahedral material.

We now introduce a quantitative measure for comparing a local configuration of atoms to the ideal structure of polytope $\{3,3,5\}$. Nelson and Widom [Nelson

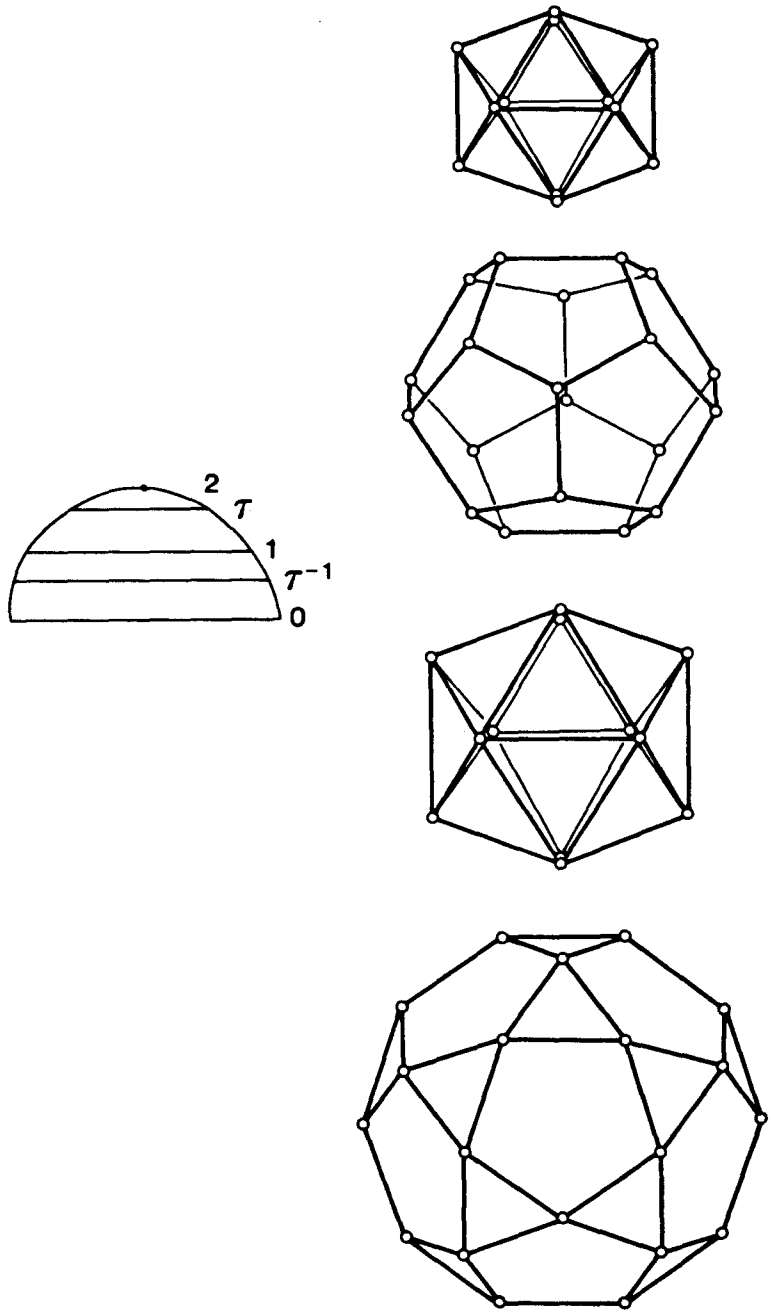

Figure 4.2 Polytope $\{3,3,5\}$ seen in an exploded view as a series of 3-dimensional cuts through the 4-dimensional sphere S^3 (represented as a semicircle on the left). As the fourth coordinate, z, varies from 2 to 0, the cuts reveal a point (z=2), an icosahedron ($z=\tau$), a dodecahedron (z=1), a larger icosahedron ($z=\tau^{-1}$), and an icosidodecahedron (z=0).

and Widom, 1984] proposed that a given atom and its nearest-neighbors be projected onto the surface of the 4-dimensional sphere S^3 based at the site of interest. This projection is then compared to a polytope $\{3,3,5\}$ of the same radius. A quantitative measure of how closely these two structures agree can be made by comparing the expansion coefficients of the projected particle density $\rho(\hat{u})$ in terms of the 4-dimensional spherical harmonics Y_{n,m_1,m_2}

$$\rho(\hat{u}) = \sum_{n,m_1m_2} Q_{n,m_1m_2} Y^*_{n,m_1m_2}(\hat{u}), \tag{4.1}$$

where $\hat{u}$ is a point on the sphere S^3, n is the principal quantum number and $-n/2 \leq m_1, m_2 \leq n/2$. Since the 4-dimensional spherical harmonics are orthonormal on the sphere S^3, we can invert to find the expansion coefficients

$$Q_{n,m_1m_2} = \int d\Omega_{\hat{u}}\ Y_{n,m_1m_2}(\hat{u})\ \rho(\hat{u}).$$

The order parameter Q_{n,m_1m_2} can be compared to that of the ideal icosahedral structure of polytope $\{3,3,5\}$, to determine the degree of local icosahedral ordering present at the site. Nelson and Widom [Nelson and Widom, 1984] have constructed a quantity analogous to the scattering structure factor for polytope $\{3,3,5\}$. As with Bragg scattering from an ordinary crystal, there is a discrete set of reciprocal lattice vectors having non-zero scattering intensity from polytope $\{3,3,5\}$. The first such non-zero scattering amplitude is for n=12 [Nelson and Widom, 1984], so that Q_{12,m_1m_2} is a special term in the density expansion (4.1). Because of this, we shall use Q_{12,m_1m_2} $(-6 \leq m_1, m_2 \leq 6)$ as our local icosahedral order parameter.

4.4 Disclination Lines

The experimentally observed crystalline structures that are the most similar to an ideal predominantly icosahedral material are the intermetallic Frank-Kasper (FK) phases. The FK phases are simply defined as topologically close-packed intermetallic compounds with exclusively tetrahedral interstices between the atoms [Sinha, 1972]. Of course, many of these tetrahedra are distorted and irregular.

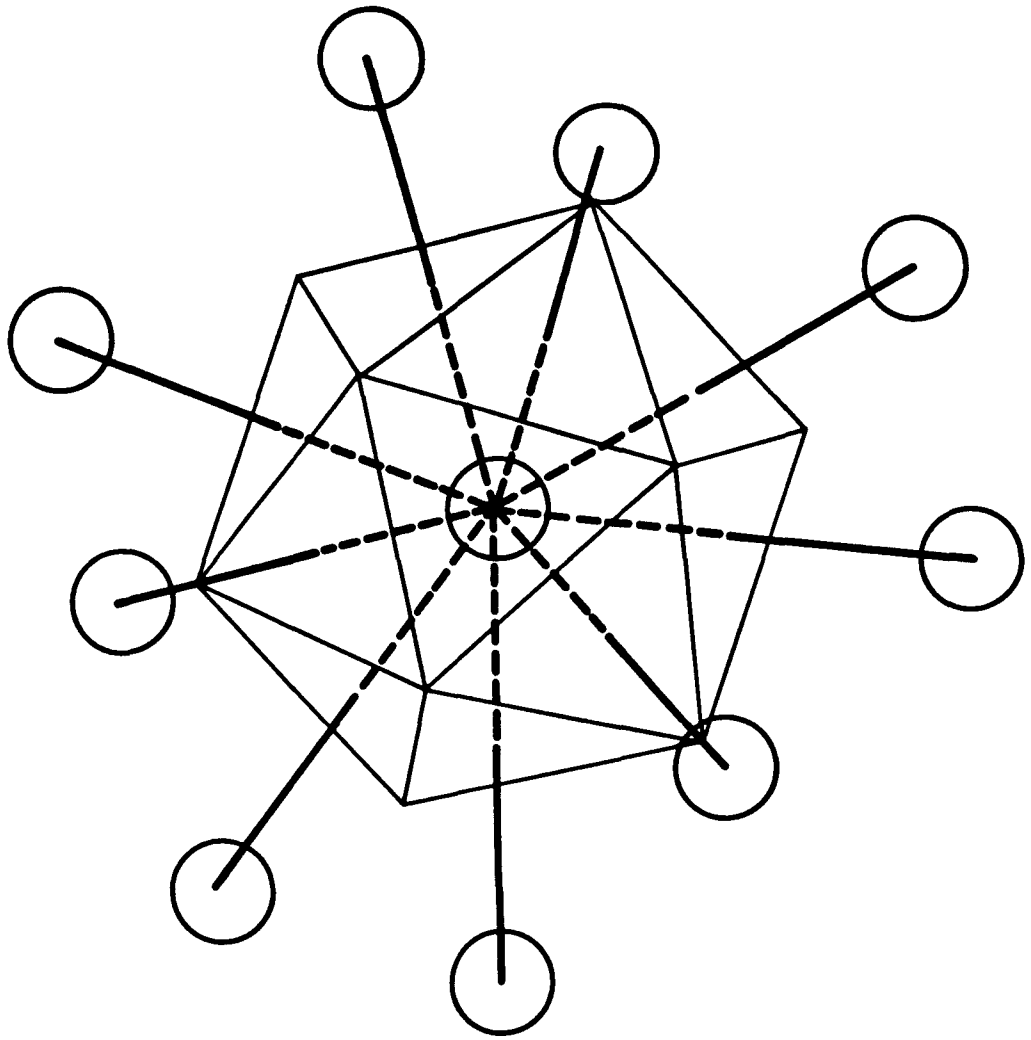

Figure 4.3 An icosahedral cluster of atoms and the Voronoi construction for the central atom.

One can define nearest-neighbor coordination polyhedra using the Voronoi method in real space. Figure 4.3 is a nearest-neighbor Voronoi construction for an atom in an icosahedral cluster of atoms. With this construction, one can uniquely define the nearest-neighbors of a given atom. Once the nearest-neighbors of the atom are defined, the coordination polyhedron is formed by the lines joining the centers of atoms in the nearest-neighbor shell. Because the FK phases have exclusively tetrahedral packing configurations, one finds that all faces of the nearest-neighbor polyhedra will be triangular (although the triangles may be irregular), and that the polyhedron can be broken up into a collection of tetrahedra [Sinha, 1972]. In the case of Figure 4.3, the central atom is a common point for the twenty tetrahedra that make up the nearest-neighbor coordination polyhedron. Each nearest-neighbor bond is a common edge for a discrete number of tetrahedra. In the case of an icosahedral coordination, there are exactly five tetrahedra wrapped around every nearest-neighbor bond emerging from the central atom.

Frank and Kasper identified four different kinds of coordination polyhedra in the FK phases; coordination number 12 (CN12), CN14, CN15 and CN16 [Frank and Kasper, 1958; 1959]. In all of these coordination polyhedra there are only two kinds of nearest-neighbor bonds, those surrounded by either five or six tetrahedra. Some metastable structures also involve nearest-neighbor bonds surrounded by only four tetrahedra. These three types of nearest-neighbor bonds are illustrated in Figure 4.4. Bonds surrounded by four or six tetrahedra are not found in icosahedral environments and are in the minority in the FK structures. These "anomolous" bonds are referred to as disclinations since they represent a rotational anomaly in the structure (i.e., a deviation from five in the number of tetrahedra around the bond). Since one tetrahedron is either present or missing along these bonds, they are referred to as $\mp 72°$ disclination lines ($72°$ being the dihedral angle of a regular tetrahedron).

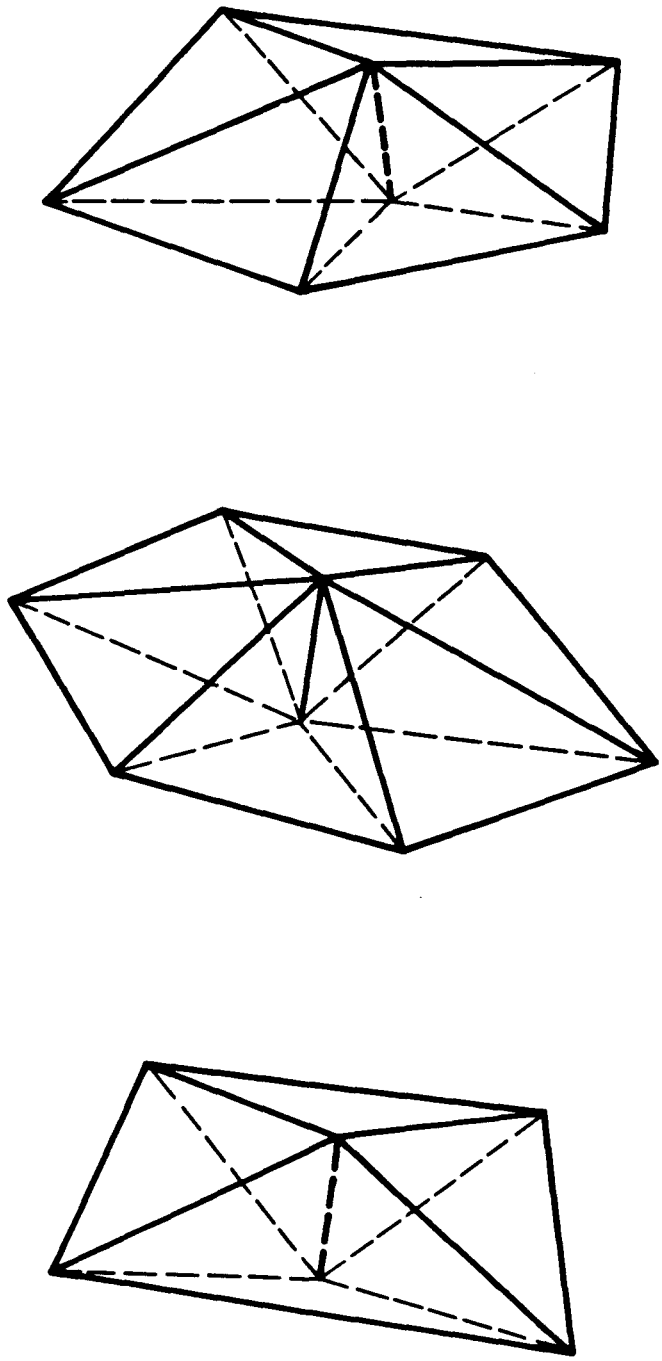

Figure 4.4 The three types of nearest-neighbor bonds; 0°, -72° (extra tetrahedron inserted around the bond) and +72° (missing tetrahedron) disclinations [after Nelson, 1983b].

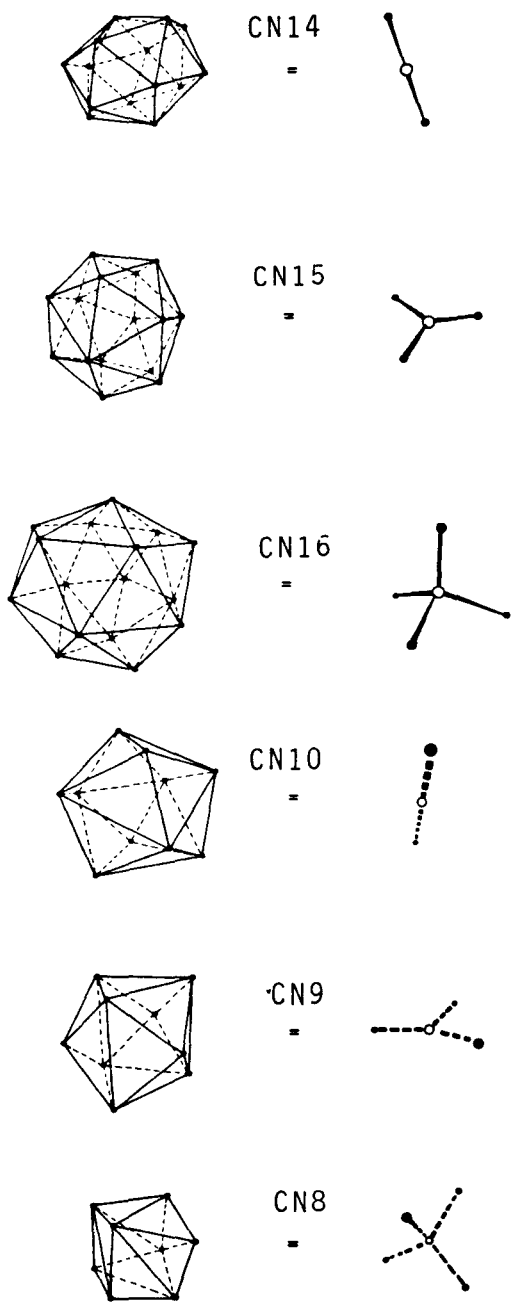

Figure 4.5 The Kasper polyhedra (CN14, CN15, CN16) and Bernal holes (CN10, CN9, CN8) along with their representations in terms of disclination lines [after Nelson, 1983b].

All of the coordination polyhedra commonly found in known intermetallic compound crystal structures and in metallic glass models are tabulated in Figure 4.5. These polyhedra have an equivalent representation in terms of the anomalous disclination lines, also shown in Figure 4.5. It can be shown that these lines form continuous networks that permeate the solid [Nelson, 1983b]. An example of such a continuous network is that for the A15 (A_3B) structure (Figure 4.6). Here, the A atoms sit in CN14 sites, whereas the B atoms are all in CN12 sites. The disclination lines that run through the A atom coordination polyhedra form three mutually perpendicular non-intersecting arrays that end only at the surfaces or grain boundaries of the crystal. An icosahedron is composed of twenty distorted tetrahedra which meet at a single point. All of the nearest-neighbor bonds of the central atom are surrounded by five tetrahedra, so a disclination line must connect only two atoms that are not in icosahedral symmetry sites. Disclination lines, in fact, provide an alternative shorthand notation for describing the structure of metals.

The physical picture of a predominantly icosahedral material is now complete. The icosahedral order parameter Q_{12} gives a quantitative measure of the degree of local icosahedral ordering in the material. Regions of strong icosahedral ordering are broken up by disclination lines, which link atoms that are not in icosahedral environments. In the next chapter we shall develop a theory for the thermodynamic properties of a predominantly icosahedral material.

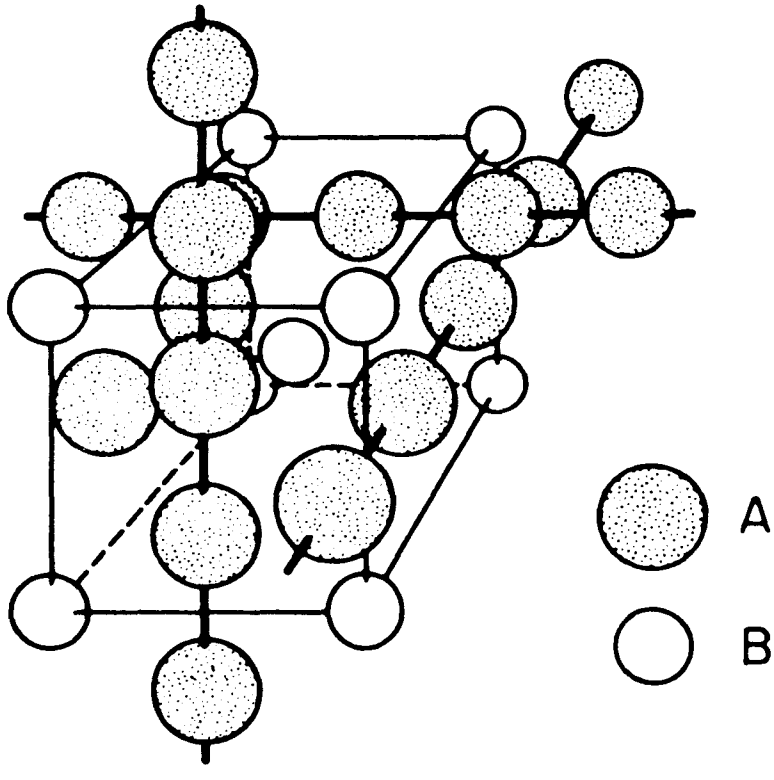

Figure 4.6 The A15 (A_3B) structure with disclination lines running through the A atoms in three mutually perpendicular directions [after Sinha, 1972].

Chapter 5 Thermodynamics of a Predominantly Icosahedral Material

To model the physics of a predominantly icosahedral material (PIM), we shall draw upon its close analogy to the Ginzburg-Landau theory of type II superconductors. Once this analogy has been established, the PIM theory will have been seen to have many non-linearities, which make it nearly impossible to attack analytically. A numerical study of the model is performed by discretizing the theory, using the well-established techniques of lattice gauge theory.

An alternative derivation of the field theory of a predominantly icosahedral material may be found in Appendix II. This appendix elaborates on the theory presented in Sections 5.1 and 5.2.

5.1 Ginzburg-Landau Theory of Superconductivity

In the Ginzburg-Landau (GL) theory of superconductivity, the order parameter is the complex scalar electron condensate wave function ψ. The external field that interacts with the condensate is the magnetic field $\vec{H}$. The free energy functional for a superconductor is [Tinkham, 1975],

$$F = \frac{1}{2m^*} \mid (-i\hbar\nabla - \frac{e^*}{c}\vec{A})\psi \mid^2 + \alpha \mid \psi \mid^2 + \frac{\mid \vec{H} \mid^2}{8\pi} + \gamma \mid \psi \mid^3 + \frac{1}{2}\beta \mid \psi \mid^4 + \ldots, \quad (5.1)$$

where m^* and e^* are the effective mass and charge of the electrons, $\vec{A}$ is the vector potential associated with the field $\vec{H}$, and α, β, γ are, in general, temperature-dependent parameters. This energy expansion is valid near the phase transition where $\mid \psi \mid$ is small.

Superconductors are characterized by their diamagnetic properties. This is observed through the Meissner effect, i.e., the sudden exclusion (either total or partial) of magnetic flux from the bulk of the material as it becomes superconducting. Type I materials are characterized by their perfect diamagnetism in the bulk. A type II superconductor exists in the mixed state, characterized by a partial penetration of

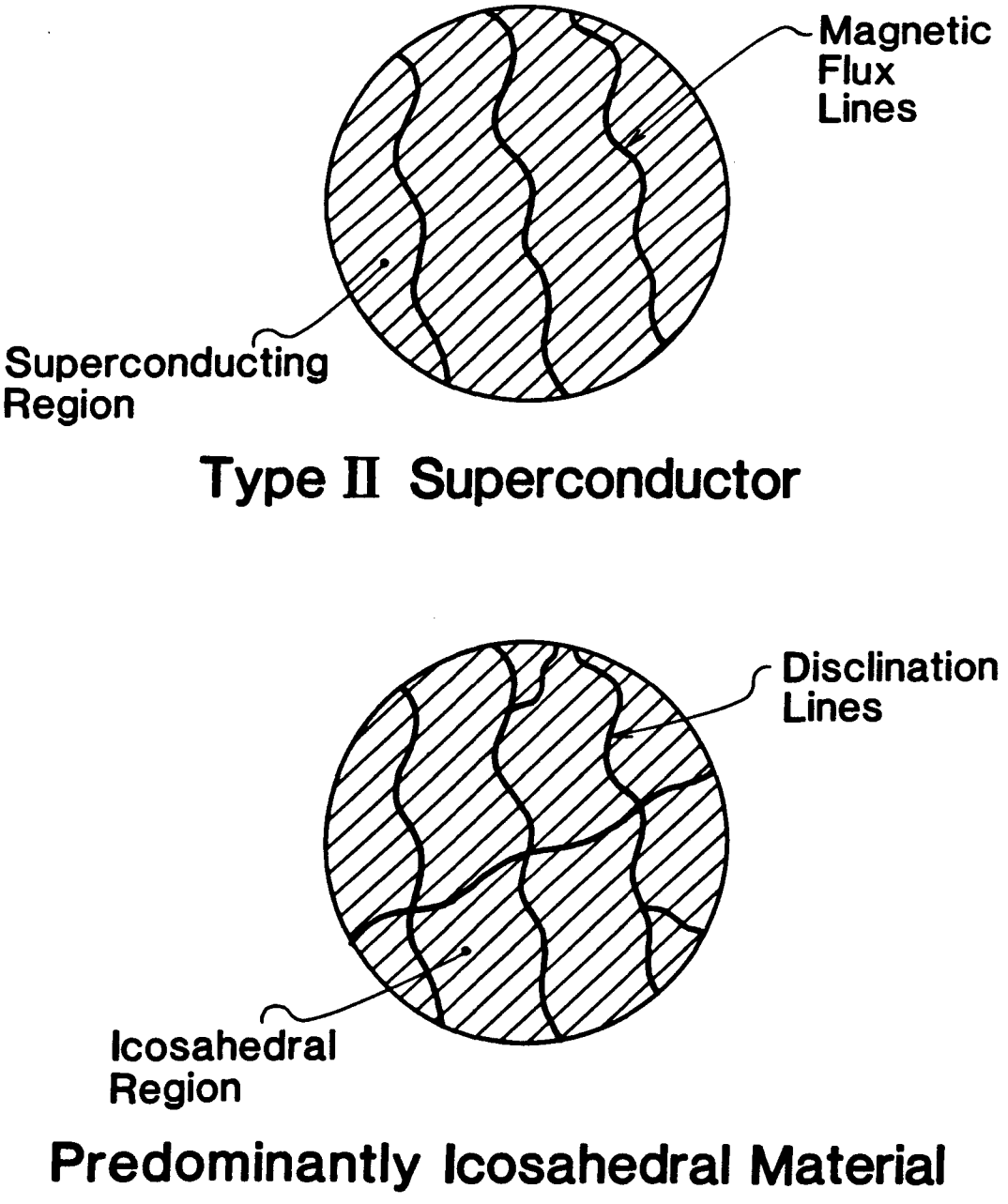

Figure 5.1 Comparison of the type II superconductor and a predominantly icosahedral material.

magnetic flux into the bulk [Rose-Innes and Rhoderick, 1978a]. Although Ginzburg-Landau theories are ordinarily used to describe second order phase transitions, the free energy expansion of Equation (5.1) will exhibit a first order phase transition in the presence of an external magnetic field [Rose-Innes and Rhoderick, 1978b].

5.2 Ginzburg-Landau Theory of a Predominantly Icosahedral Material

Figure 5.1 illustrates the analogy between a type II superconductor described by the GL theory and our physical picture of a predominantly icosahedral material. Both theories contain order parameters to describe the long-range order. This order is disrupted by linear defects on which the icosahedral order parameter goes to zero. Table 5.1 outlines the detailed analogy between the GL and PIM theories.

Using Table 5.1 as a guide, an energy expansion for the PIM can be written down in analogy with Equation (5.1)

$$F = \frac{1}{2}\sum_{m} \mid D_\mu Q_{12,m} \mid^2 + \alpha \sum_{m} \mid Q_{12,m} \mid^2 + \frac{1}{3} \mid F_{\mu\nu} \mid^2 + \text{higher order terms.} \quad (5.2)$$

The first term in Equation (5.2) involves the covariant derivative,

$$D_\mu Q_{12,m} = \sum_{m'} [\delta_{m,m'}\partial_\mu - i\kappa(A_\mu)_{m,m'}]\, Q_{12,m'},$$

where κ is the coupling constant between the order parameter and disclination line fields, and m represents the set $\{m_1, m_2\}$. In analogy with the vector potential of the magnetic flux lines, A_μ is the vector potential associated with the disclination lines. The third term in Equation 5.2 accounts for the self-energy of the disclination line network. As with the electromagnetic contribution to the total energy of a type *II superconductor, this term involves the absolute square of the tensor,*

$$F_{\mu\nu} \equiv \partial_\mu A_\nu - \partial_\nu A_\mu - i\kappa[A_\mu, A_\nu].$$

In a superconductor, the commutator between different components of the vector potential is zero; i.e., the magnetic field is Abelian, meaning that magnetic flux lines

Table 5.1 The formal analogy between the Ginzburg-Landau theory of superconductivity and the gauge field theory of predominantly icosahedral materials (PIM).

Ginzburg-Landau	PIM
Condensate Wavefunction, ψ	Icosahedral Order Parameter, Q_{12,m_1m_2}
Abrikosov Flux Lattice	Disclination Line Network
Meissner Effect	Disclination Flux Exclusion

PIM will be expelled (at least partially). This exclusion of disclination line flux will permit long-range ordering to occur in the icosahedral order parameter field. Thus the Meissner effect will be analogous to a transition from a high-temperature disordered PIM (or liquid) to a low-temperature phase with enhanced short-range icosahedral order.

A more formal derivation and explanation of Equation (5.2) may be found in Appendix II.

5.3 The Discretized Theory

We can investigate the equilibrium thermodynamics of a predominantly icosahedral material, starting from the partition function

$$Z = \sum_{\text{states}} e^{-\beta \int d^3x \, F(Q_{12,m}(\vec{x}),\vec{A})},$$

where the sum is over all possible configurations of the order parameter and disclination line fields. This quantity can be effectively calculated using a Monte Carlo sampling technique, since only those field configurations near the equilibrium configuration will make significant contributions to the sum. To implement the Monte Carlo sampling technique, the energy expansion in Equation (5.2) must be made discrete. This is accomplished by using the techniques of lattice gauge theory.

In recent years, lattice gauge theories have been developed as a means of studying the complicated non-linear properties of the quark-gluon plasma [Rebbi, 1983]. In this approach we use a discrete space-time approximation, with the matter field placed on the lattice sites of a 4-dimensional hypercubic lattice and the gauge field transporters on the links between the sites. We determine a discretized energy functional in terms of the lattice site and link variables. The partition function and any thermodynamic quantities and order parameters can then be calculated approximately by means of Monte Carlo sampling.

In this approach we use a discrete space-time approximation, with the matter field placed on the lattice sites of a 4-dimensional hypercubic lattice and the gauge field transporters on the links between the sites. We determine a discretized energy functional in terms of the lattice site and link variables. The partition function and any thermodynamic quantities and order parameters can then be calculated approximately by means of Monte Carlo sampling.

The discrete version of the PIM theory can be constructed in direct analogy with lattice gauge theory. A discrete cubic lattice is introduced with the icosahedral order parameter (Q_{12}) on the lattice sites and the disclination line potential (A) on the links between the sites. Next, a discretized version of Equation (5.2) is written in terms of the lattice site and link variables.

The covariant derivative term of Equation (5.2) can be easily expressed as the difference between the order parameter at site j and the order parameter at site i transported back to j (under the influence of the neighboring disclination lines). A simple form for this is

$$| D_\mu Q_{12,m_1m_2}(\vec{x}_j) |^2 \longrightarrow \frac{1}{a^2} \sum_{i \text{ n.n. } j} | Q_{12,m_1m_2}(\vec{x}_j) - U_{ji} Q_{12,m_1m_2}(\vec{x}_i) |^2,$$

where a is the lattice parameter, and the sum is taken over the nearest-neighbors i of site j. The quantity $U_{ji} \equiv e^{iA(\frac{x_i+x_j}{2})a}$ is called a transporter because multiplication by this quantity represents the effect of the disclination lines on the order parameter as it is moved from x_i to x_j. The transporter embodies the effect of the disclination lines on the order parameter as the order parameter is moved about in space.

Following Wilson [Wilson, 1974], the third term in Equation (5.2) can be written as a sum over plaquettes (i.e., elementary squares of links in the lattice) of a function of disclination field transporter products

$$| F_{\mu\nu} |^2 \longrightarrow \sum_{\text{plaquettes } \square} (1 - \text{Re Tr}(U_\square)),$$

where $U_\square$ is the product of transporters around an elementary square of the lattice, and the trace can be taken in one of several matrix representations of the transporters.

The discretized energy expansion finally becomes

$$F = \sum_{\substack{\langle i,j \rangle \text{ n.n.} \\ m_1 \; m_2}} | Q_{12,m_1m_2}(\vec{x}_j) - U_{ji} Q_{12,m_1m_2}(\vec{x}_i) |^2 + \alpha \sum_{m_1 \; m_2} | Q_{12,m_1m_2} |^2 + \frac{1}{3} \sum_{\text{plaquettes } \square} f(U_\square) + \text{higher order terms}, \tag{5.3}$$

where $f(U_\square)$ is a function (to be chosen) of the trace of a plaquette product of disclination field transporters.

5.4 Phase Structure of the Predominantly Icosahedral Material

A Monte Carlo sampling of all the possible configurations of the order parameter and frustration fields in a calculation of the partition function would be astronomically time consuming. In order to reduce the number of available states, and the computational labor, we are compelled to reduce the number of degrees of freedom available to the site and link variables. These simplifications are physically motivated.

As noted in Section 4.4, all of the defect lines present in topologically close-packed intermetallic compounds are simple $-72°$ disclinations (i.e., one tetrahedron has been added to a nearest-neighbor bond). Analysis of the Bernal holes in metallic glasses show that in addition to the $-72°$ disclinations, there are mainly $+72°$ disclination lines present [Nelson, 1983a; 1983b]. With these observations in mind, we can restrict the number of possible defect lines to just the disclinations, and then among those we shall consider only the $0°$ (i.e., no disclination) and $\pm 72°$ disclination lines. The spectrum of self energies per unit length that we have chosen for the disclinations is given in Table 5.2. The energy-per-unit length of a Kasper ($-72°$) disclination line is called E_1. Since the Bernal ($+72°$) disclination line is

Table 5.2 Values of the energy-per-unit length of all disclination lines used in the Monte Carlo simulations.

Disclination Line	Energy-per-Unit Length (units of E_l)
0°	0
−72° (Kasper)	1.0
+72° (Bernal)	1.1

found in metastable structures, it is given a slightly higher (10%) energy-per-unit length. This spectrum of self-energies represents our choice of the function f in Equation (5.3).

By considering only the 0° and ±72° disclination lines, and ignoring all the other possible defect lines discussed in Appendix II, we hope to reduce the number of degrees of freedom available to the system, and still retain the essential physics of a predominantly icosahedral material.

As a consequence of considering only disclination line defects, we can also make an important simplification to the order parameter field. Since disclinations are defect lines labelled in the form $(l, l) \in Y' \times Y'$ (where Y' is the double group of the icosahedron) [Nelson and Widom, 1984], they can rotate the order parameter into only a limited number of new states. Hence, it is not necessary to include the entire manifold of the order parameter field in the computation. Because of this, we shall simplify the manifold of the order parameter to be just the group Y'.

In the Monte Carlo simulations of a predominantly icosahedral material, we shall consider the order parameter and defect line fields to be independent stochastic variables. In an effort to disentangle the physics of the defect lines from that of the icosahedral order parameter, we shall consider a predominantly icosahedral material with only defect lines, ignoring the order parameter. This model describes a material with varying densities of icosahedral clusters, ignoring the possible correlations in the orientation of neighboring clusters. It is described by just the third term in Equation (5.3).

The numerical model of a predominantly icosahedral material is now complete. On the lattice sites is an icosahedral order parameter field, which can take on values given by elements of the discrete double group of the icosahedron Y'. Between the sites there exist disorder field transporters whose plaquette products $U_\square$ are also elements of the group Y'. We have used a Monte Carlo sampling algorithm to

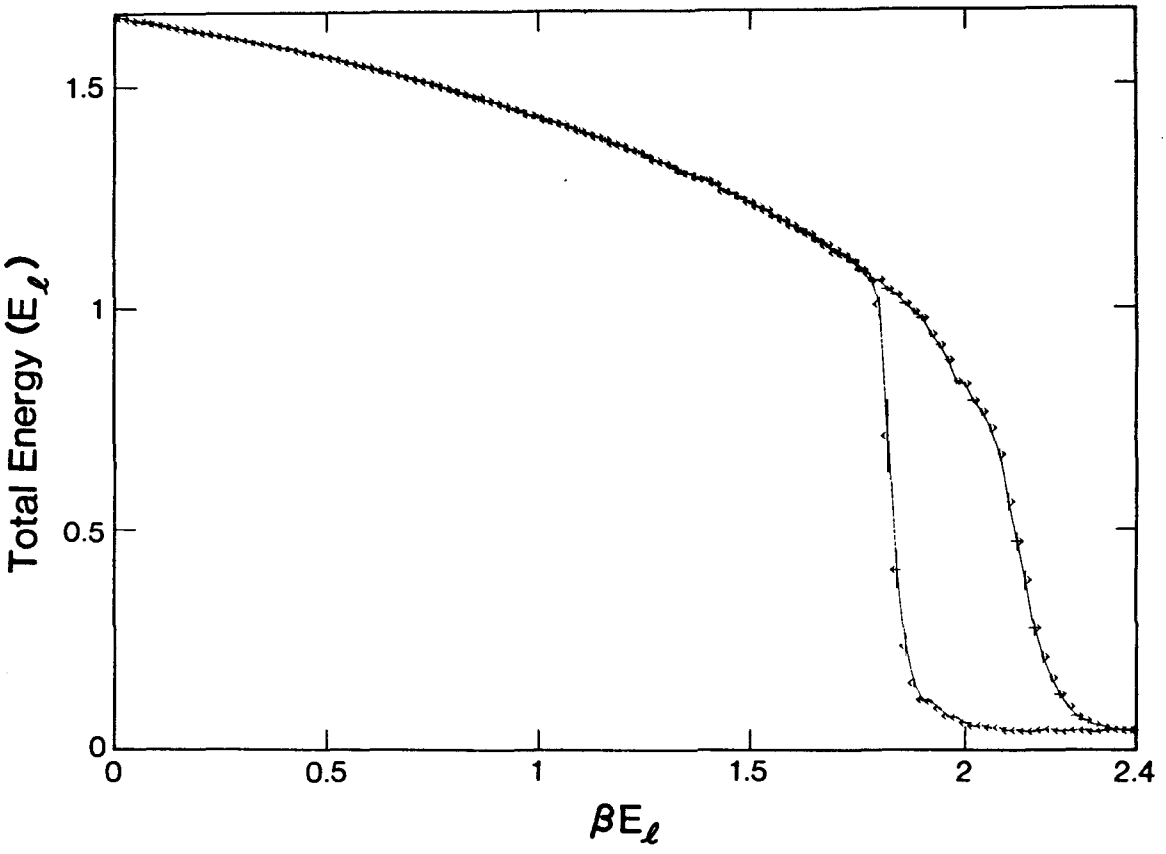

Figure 5.2 Cyclic annealing treatment of a 16^3 lattice with only disclination lines present. The internal energy of the disclination lines (in units of E_l) is plotted against the dimensionless inverse temperature $E_l/k_B T$.

study the phase structure of this model material.

5.5 Results

In this thesis, we shall consider only the simplest version of the PIM model. Consider a PIM with only disclination lines present (i.e., ignore the icosahedral order parameter Q_{12}). This model describes the density of icosahedral short-range order in the PIM. By ignoring the icosahedral orientational order parameter Q_{12}, we will not see a phase transition to the long-range orientationally ordered icosahedral solid. This long-range ordered solid is expected to be either an equilibrium Frank-Kasper phase or the icosahedral phase.

Nevertheless, this simple model already displays some interesting and non-trivial behavior. The presence of a disclination line means that a set of atoms on that line are not surrounded by an icosahedral cluster. Hence, the disclination line density is a measure of the extent of local icosahedral site symmetry in the material. In what follows, we shall examine a PIM described by only the third term in Equation (5.3).

In order to distinguish two phases of the model, which are separated by a transition, we must evaluate several numerical order parameters. The simplest order parameters to evaluate are the average internal energies calculated in Equation (5.3). We examine the first and third terms in Equation (5.3) separately. The third term of Equation (5.3) is just the energy associated with the defect line threading through the plaquette, averaged over the entire lattice.

To deduce the phase structure of the PIM model, we must evaluate order parameters that distinguish all of the phases. The phase transitions are then recognized as points where the order parameter or its derivatives are discontinuous. These phase transitions can be found most conveniently by performing a cyclic annealing treatment on the model and monitoring the order parameter and its temperature derivative. Once a phase transition is found, it can be isolated and characterized

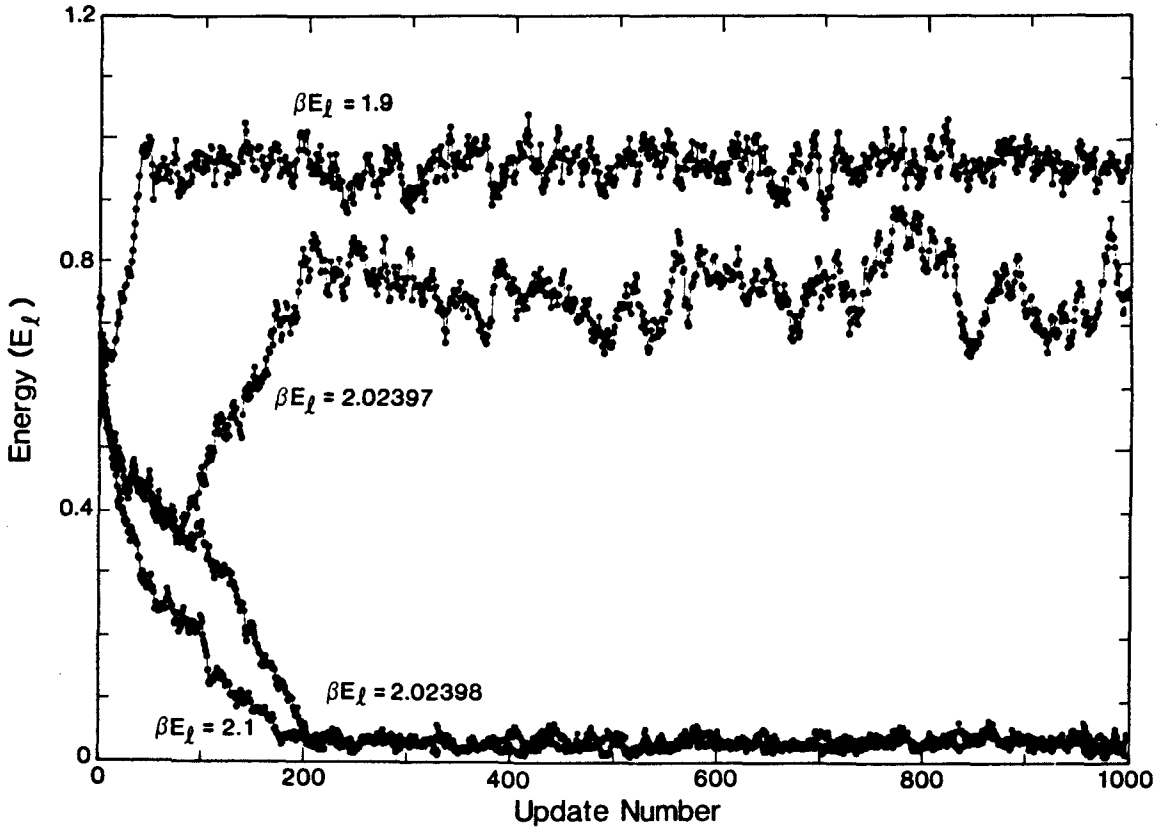

Figure 5.3 Disclination line internal energy (in units of E_l) is plotted against Monte Carlo update number for a 16^3 lattice with only disclination lines on the links. These annealing treatments are carried out both above and below the transition temperature.

by performing mixed initial configuration runs near the transition temperature.

Figure 5.2 shows a cyclic annealing run between βE_l ($\equiv E_l/k_B T$) = 0 to 2.4 and back to 0. The order parameter is the internal energy (in units of E_l) due to just the disclination lines (i.e., the third term in both Equations 5.1 and 5.3). In this version of the model the disclination lines alone produce the observed first order transition around $\beta E_l \simeq 2$. The transition was isolated by starting the system in a mixed initial configuration. A half block of the lattice links were set to the identity element (i.e., no disclinations are present through the plaquettes) and the links in the other half block were assigned randomly. The system is then annealed for a long period of time until the entire lattice settles into one of the two competing states. Such annealing treatments have been used to place limits on the transition temperature, $2.02397 < (\beta E_l)_c < 2.02398$ (see Figure 5.3).

The high-temperature phase is characterized by a high density of disclination line defects. This high density of defects implies that many of the atomic sites are not icosahedral symmetry sites. This high-temperature phase may then represent a liquid or cubo-octahedral crystalline solid. On the other hand, the low-temperature phase has very few disclination lines, implying that most of the atoms sit in icosahedral environments. However, it is known that a finite density of disclination lines must always be present in a real material [Nelson, 1983b]. Nelson estimates that the mean number of tetrahedra around the nearest-neighbor bonds of a real material must be approximately 5.1, rather than 5.0 as in a disclination-free phase. The low-temperature phase of the predominantly icosahedral material model does not satisfy this requirement. In fact, this freezing transition is equivalent to studying the transition from a randomly curved space (high-temperature phase) to the uniformly curved space of polytope $\{3,3,5\}$ (low-temperature, disclination-free phase). A more realistic low-temperature phase will be found if an "external curvature field" is applied to the system. This must be done to ensure that the ground state phase

has an average of 5.1 tetrahedra surrounding the nearest-neighbor bonds.

The model predicts a phase transition from a high-temperature (icosahedrally) disordered phase to a low-temperature phase with extensive icosahedral site symmetry. Although the low-temperature phase cannot be said to be the icosahedral phase, it does have a high density of CN12 coordination sites. The identification of an icosahedral phase will come only when the correlations of both the disclination lines and the icosahedral order parameter are examined. With these reservations, in Chapter 6 we shall compare the calculated phase transition of a PIM with icosahedral phase formation from the melt, and fix a value for the parameter E_1 in the theory.

Chapter 6 Comparison of Theory and Experiment

6.1 Fixing Theoretical Parameters

By comparing the results of annealing treatments on the model predominantly icosahedral material (PIM) with experimental results for icosahedral phase formation, we can fix the parameter E_l. The first order phase transition observed in the PIM model is qualitatively similar to the formation of the icosahedral phase from a rapidly quenched liquid metal. Anlage et al. [Anlage et al., 1987] have estimated that the peritectic formation temperature of icosahedral Al-Ru is about 1500K. Using the calculated value of $(\beta E_l)_c$, we find that $E_l \simeq \frac{1}{4}$ eV/nearest-neighbor bond distance is the energy-per-unit length of a Kasper disclination line in Al-Ru.

The latent heat of the freezing transition can be estimated from Figure 5.3. We find that $\Delta H_c \simeq 0.8 E_l$ (since $\Delta(PV) = 0$). With the above value of E_l, the latent heat amounts to about 0.2 eV/site in Al-Ru. Richards' rule [Swalin, 1962] says that the latent heat per site for ordinary melting of a typical elemental metal is about 0.2 eV/site. This agreement is fortuitous for several reasons. First, the absence of disclination lines in the low-temperature phase means that it has an unphysically low entropy. Correcting this will decrease the calculated value of ΔH_c. In addition, the phase transition does not include the contribution that will come from the long-range ordering of the icosahedral order parameter Q_{12}. When this is included, it will increase the calculated value of ΔH_c.

6.2 Summary and Conclusions

There is substantial experimental and theoretical evidence for the existence of icosahedral local order in many metallic systems (both solid and liquid). Icosahedral clustering was conceived as a speculative explanation for the supercooling properties of liquid metals and the formation of metallic glasses. It received experimental substantiation through a number of different observations, including the identifica-

tion of icosahedral coordination shells in large unit cell crystals and the existence of rapidly quenched alloys with icosahedral point group symmetry extending over substantial length scales. Computer simulations of small metallic clusters have also provided clear evidence for local icosahedral ordering.

We have observed the formation of a long-range ordered icosahedral phase from a rapidly quenched liquid metal. In an attempt to explain this observation, we propose a model predominantly icosahedral material (PIM). This PIM is endowed with short-range icosahedral order just like that believed to exist in supercooled liquid metals. To describe the structure of a predominantly icosahedral material, it is most convenient to replace the atomic structure with the equivalent coordination polyhedra and then analyze the statistical character of these polyhedra. One then finds that most of the nearest-neighbor bonds (which pass through the face centers of the coordination polyhedra) are defined by five tetrahedral clusters of atoms that share a common edge. Most of the remaining nearest-neighbor bonds are surrounded by four or six such tetrahedral clusters. The latter, anomolous bonds, are called disclination lines and they form a continuous network, which permeates the material. We now regard the predominantly icosahedral material as a uniform "icosahedral backround" (where the nearest-neighbor bonds are the common edge of five tetrahedral clusters) interrupted by disclination line defects.

The theory can be formalized by introducing Nelson's local icosahedral order parameter. The local atomic configuration is projected onto the surface of the four-dimensional sphere S^3 and compared to the ideal local icosahedral structure of polytope $\{3,3,5\}$. The local icosahedral order parameter takes on values from a limited manifold of states. By physical arguments, we find that the $\pm 72^\circ$ disclinations are the most interesting defects in a predominantly icosahedral material.

Drawing on ideas from field theory, we can replace the line defects by a disorder field. A line defect is uniquely described by the product of disorder field transporters

on a loop around the line. The field theory reduces the structure of a PIM to an order parameter field and an associated disorder field.

By analogy with the well-known gauge theories of physics (in particular, the Ginzburg-Landau theory of superconductivity), we propose a free energy functional to describe the PIM. Once the theory is constructed, it is then straightforward to investigate the equilibrium thermodynamic properties of the system by means of a modified Monte Carlo lattice gauge theory analysis. The theory predicts a first order phase transition from a high-temperature (icosahedrally) disordered phase to a low-temperature phase with a high density of icosahedral atomic environments. Because the low-temperature phase has some of the properties of an icosahedral phase, we use the results of the theory to give a qualitative description of the liquid-to-icosahedral phase freezing transition. The energy-per-unit length of a Kasper disclination line in Al-Ru is found to be approximately $\frac{1}{4}$ eV/nearest-neighbor bond distance.

Appendix I The Curved Space Description of Amorphous Materials

Over the past 10 years, a conceptual theory of metallic glass structure has been developed, based on the axiom of local icosahedral clustering in metals. The development has been led by the seminal works of Sadoc and Kléman. Their ideas about the structure of noncrystalline materials can be (quite generally) summarized as follows [Sadoc, 1981; Kléman and Sadoc, 1979];

1. There is a well defined local order in noncrystalline materials.
2. There is an incompatibility between the symmetry of this local order and the properties of Euclidean space (i.e., topological "frustration").
3. Appropriately chosen curved spaces can be tesselated (i.e., filled without leaving any gaps or holes) with a unit cell having the forbidden local order symmetry.
4. The disorder which is present in noncrystalline solids is due to the projection (i.e., flattening process) from curved space to Euclidean space.

In the particular case of an icosahedral metallic glass structure, the well defined local order is that of an icosahedral cluster. An icosahedral cluster of thirteen atoms is energetically favored over similarly sized clusters of cubo-octahedral symmetry [Frank, 1952]. The incompatibility of icosahedral symmetry with the properties of Euclidean space is well known [Hamermesh, 1962; Kittel, 1976; Burns, 1985]. The competition between a minimum energy configuration of atoms and the necessity of filling space without leaving holes is a form of topological frustration, and can force the material into a noncrystalline state.

Kléman and Sadoc [Kléman and Sadoc, 1979] recognized that an appropriately chosen curved space could be tesselated with an icosahedral "unit cell." In three-dimensional Euclidean space, five perfect tetrahedra wrapped around a common edge do not close, but leave a deficit angle of about 7° (see Figure 1.3). By choosing the appropriate radius, the surface of the sphere S^3 (which is a finite, curved three-dimensional space) can be curved just enough to close up this deficit angle

and produce a perfect icosahedral tesselation. The curved space that Sadoc chose is a decoration of the four-dimensional sphere S^3 with a collection of vertices, each of which has a perfect icosahedral coordination shell. Its name, polytope $\{3,3,5\}$, describes in Schoenflies notation a regular object having five tetrahedra ($\{3,3\}$) wrapped around every nearest-neighbor bond (see Figure 4.2). In fact, one can use the mean number of tetrahedra wrapped around a nearest-neighbor bond as a measure of the local "curvature" of space. Polytope $\{3,3,5\}$ represents the ideal frustration-free packing of equal size spheres with minimum potential energy (assuming two-body, central forces) and will serve as a standard to which we compare the local structure of an icosahedral metallic glass.

The atomic structure of a real metallic glass can be obtained by projecting the ideal structure of polytope $\{3,3,5\}$ onto Euclidean space. Kléman and Sadoc [Kléman and Sadoc, 1979] proposed that this projection could be accomplished by introducing defect structures to "de-curve" the space (i.e., to change the average number of tetrahedra wrapped around the nearest-neighbor bonds). These defects are called disclination lines and are coincident with nearest-neighbor bonds that involve a deviation from five in the number of tetrahedra wrapped about the bond (see Figure 4.4). In an icosahedral coordination shell, all of the nearest-neighbor bonds emanating from the central atom are surrounded by five tetrahedra. A $-72°$ ($+72°$) disclination line corresponds to that nearest-neighbor bond being surrounded by six (four) tetrahedra ($72°$ being the dihedral angle of a regular tetrahedron). By adding an appropriate density of disclination lines, one can effectively change the local curvature of space and "flatten out" polytope $\{3,3,5\}$ into Euclidean space.

Thus in the Sadoc-Kléman view, a metallic glass is described as a set of partially overlapping polytopes flattened out into Euclidean space by the introduction of disclination lines. This flattening process will destroy any translational order in the final projection, but it will preserve orientational order. Thus, in its simplest

form, the Sadoc-Kléman theory is naturally suited for orientationally ordered non-crystallographic materials such as the icosahedral phase, but not for a more highly disordered structure like a metallic glass. For a review of work on the curved space description of amorphous materials, see the paper by Venkataraman and Sahoo [Venkataraman and Sahoo, 1985].

Appendix II A Field Theory of Local Icosahedral Order in Metals

In this appendix we shall develop a structural description of predominantly icosahedral materials by focusing on the most disordered metallic solid, the metallic glass. A description of the structure of a metallic glass in terms of the detailed arrangement of all the atoms is an overwhelmingly complex task, and once it is completed, may not provide any unique insight about the material. We must find a way of organizing the structure of the glass to reduce the number of degrees of freedom needed to specify it completely. In this appendix, our premise is that a predominantly icosahedral material can best be described as a uniform icosahedral backround whose structure is locally like that of polytope $\{3,3,5\}$. In addition, disclination line defects must be present to accomodate the difference in curvature between Euclidean space and the curved space of polytope $\{3,3,5\}$. The properties of the material are then largely determined by the interaction and dynamics of the defect lines.

We can achieve an approximate description of an icosahedral metallic glass structure by two routes, one being more physical than the other, but both using the curved space description of noncrystalline materials (see Appendix I). The first (and more physical) approach involves replacing the atomic structure with a set of nearest-neighbor polyhedra and then focusing our attention on all nearest-neighbor bonds in these polyhedra not surrounded by five tetrahedra, regarding the rest of the material as an undistorted backround. A second route is more formal and involves the use of polytope $\{3,3,5\}$ as a model of the local atomic structure in a glass. An icosahedral order parameter can be defined at every atomic site in the metal by projecting the local atomic configuration onto a sphere S^3 and comparing it with polytope $\{3,3,5\}$. We apply homotopy theory to the order parameter manifold and find a large set of stable line defects, including the familiar disclinations. Thus, by this formal route, we arrive at a more general description of the stable defects

present in a predominantly icosahedral material.

A2.1 Physical Description

Frank and Kasper [Frank and Kasper, 1958; 1959] identified a large class of compounds with exclusively tetrahedral interstices, now commonly referred to as the Frank-Kasper phases. They also identified a set of four coordination polyhedra commonly found in these intermetallic crystal structures (called CN12, CN14, CN15, CN16). These coordination polyhedra are labelled by the number of nearest-neighbors surrounding the central atom. The polyhedra contain a majority of nearest-neighbor bonds surrounded by five tetrahedra (the CN12 polyhedron has exclusively fivefold coordinated bonds emanating from the central atom). The other nearest-neighbor bonds are surrounded by six tetrahedra and hence can be identified with $-72°$ disclination lines (i.e., an extra tetrahedral wedge has been inserted around the nearest-neighbor bond). Bernal [Bernal, 1965] has analyzed the structure of monatomic hard sphere potential models of metallic glass and identified three additional common polyhedra (called the Bernal holes), CN8, CN9 and CN10. In these polyhedra, some of the nearest-neighbor bonds have had a tetrahedral wedge removed, hence they become $+72°$ disclination lines. It can be shown [Nelson, 1983] that the positive and negative disclination lines form a continuous network which permeates the structure (for an example, see Figure 4.6). Thus, to a first approximation, the atomic structure of a metallic glass can be replaced by a set of coordination polyhedra. The next approximation is to replace the polyhedra with just the disclination lines between atomic sites, regarding the fivefold nearest-neighbor bonds as "normal." The atomic structure has now been replaced with a network of lines along anomalous (i.e., non-fivefold coordinated) nearest-neighbor bonds. This system has many fewer degrees of freedom than the original structure and will serve as our physical description of a predominantly icosahedral material.

A2.2 Formal Description

One can arrive at essentially the same description of a predominantly icosahedral material as in Section A2.1 by much more formal (and general) means. Consider again the atomic structure of a metallic glass. We wish to define an icosahedral order parameter by comparing the local configuration surrounding a particular site with that surrounding the vertex of the ideal structure of polytope $\{3,3,5\}$. To do this, Nelson and Widom [Nelson and Widom, 1984] suggest that the nearby atoms be projected onto the surface of a sphere S^3 based at the site of interest and compared directly with a polytope $\{3,3,5\}$ of the same radius. A quantitative measure of how closely these two structures agree can be made by comparing the expansion coefficients of the projected particle density $\rho(\hat{u})$ in terms of the four-dimensional spherical harmonics Y_{n,m_1m_2};

$$\rho(\hat{u}) = \sum_{n,m_1m_2} Q_{n,m_1m_2} Y^*_{n,m_1m_2}(\hat{u}), \qquad \text{(A2.1)}$$

where $\hat{u}$ is a point on the sphere S^3, n is the principal quantum number and $-n/2 \leq m_1, m_2 \leq n/2$. Since the four-dimensional spherical harmonics are orthonormal on the sphere S^3, we can invert to find the expansion coefficients;

$$Q_{n,m_1m_2} = \int d\Omega_{\hat{u}}\ Y_{n,m_1m_2}(\hat{u})\ \rho(\hat{u}). \qquad \text{(A2.2)}$$

The order parameter Q_{n,m_1m_2} can be compared to that of the ideal icosahedral structure of polytope $\{3,3,5\}$, to determine the degree of local icosahedral ordering present at the site. Nelson and Widom [Nelson and Widom, 1984] have constructed a quantity analogous to the scattering structure factor for polytope $\{3,3,5\}$. As with Bragg scattering from an ordinary crystal, there is a discrete set of reciprocal lattice vectors having non-zero scattering intensity from polytope $\{3,3,5\}$. The first such non-zero scattering amplitude is for n=12 [Nelson and Widom, 1984], so that Q_{12,m_1m_2} is a special term in the density expansion of Equation (A2.1). Because

of this, we shall use the 13×13 matrix Q_{12,m_1m_2}, $-6 \leq m_1, m_2 \leq 6$, as the local icosahedral order parameter.

The object used to define the icosahedral order parameter, polytope $\{3,3,5\}$, has as its symmetry group G a 7200 element subgroup of SO(4) [Nelson and Widom, 1984]. Because any of the operations of the group G can be applied to polytope $\{3,3,5\}$ and give the same value for the order parameter, there is some internal freedom in our description. We can systematically exploit this internal freedom in two ways. First we shall use homotopy theory to enumerate the types of defects present in the icosahedral medium [Mermin, 1979; Nelson and Widom, 1984]. Then, in Section A2.4, we shall use this internal symmetry as the basis for a physical theory of the properties of an icosahedral metallic glass.

In preparation for an analysis of the stable defect structures in an icosahedral metallic glass, we must represent the order parameter manifold as a simply connected coset space. The symmetry group of the sphere S^3 is SO(4). The symmetry group of the order parameter, (A2.2), is that of S^3 reduced by the symmetry group G of polytope $\{3,3,5\}$ (i.e., this is the group of operations which will take any value of the order parameter into any other possible value). Thus the symmetry of the order parameter is the coset space SO(4)/G. The combination algebra of line defects (point defects and wall defects are not stable) in this medium is given by the fundamental group of the order parameter symmetry group [Mermin, 1979];

$$\pi_1(\mathrm{SO}(4)/\mathrm{G}) = \pi_1(\mathrm{SU}(2) \times \mathrm{SU}(2)/\mathrm{G}'),$$

where G′ is the lift of G into SU(2). Hence [Nelson and Widom, 1984],

$$\pi_1(\mathrm{SO}(4)/\mathrm{G}) = \mathrm{Y}' \times \mathrm{Y}'.$$

Thus the combination algebra for line defects in an icosahedral medium is given by the product group $\mathrm{Y}' \times \mathrm{Y}'$, where Y′ is the 60 element icosahedral point group lifted into SU(2) (i.e., the double group of the icosahedron). The elements of $\mathrm{Y}' \times \mathrm{Y}'$ can

be labelled by (l,r) where l and r are seperately chosen from the group Y′. All elements of the form (l,l) are disclinations [Nelson and Widom, 1984], and a subset of these are the $-72°$ and $+72°$ disclinations identified in Section 4.4.

We now have a formal description of the structure of an icosahedral metallic glass. At each atomic site there is an icosahedral order parameter which has been calculated by projecting the surrounding structure to S^3 and comparing it with the structure of polytope $\{3,3,5\}$. On the nearest-neighbor bonds between sites are defect lines which are parameterized by the elements of the group $Y' \times Y'$. We suspect that most of the physically relevant defect lines will be just the positive and negative disclination lines found from the analysis of intermetallic compounds and metallic glasses in terms of the Kasper polyhedra and Bernal holes respectively.

A2.3 The Disorder Field

We have found that the defect lines of our theory of an icosahedral metallic glass are parameterized by elements of the group $Y' \times Y'$. The defect lines are identified by looking at the change in the order parameter upon circumnavigating the line along a closed path C (see Figure A2.1(a)),

$$Q_{12,m_1m_2}(\vec{x}_0) \overset{\text{Traverse C}}{\longrightarrow} (l,r)\, Q_{12,m_1m_2}(\vec{x}_0), \qquad \text{(A2.3)}$$

where (l,r) $\in Y' \times Y'$ is a rotation applied to the matrix Q_{12,m_1m_2}. Suppose that the plane curve C is broken up into a series of paths along the coordinate axes (see Figure A2.1(b)). We can think of moving the order parameter around this plaquette and evaluating it at each corner. The net change in the value of the order parameter upon completing the loop parameterizes the defect line which passes through it [Toulouse and Kléman, 1976; Kléman, 1977]. Another way to look at this process is to suppose that moving from site i to site j in the direction $\hat{e}_\mu$ involves multiplication of the order parameter by a "transporter," $(U_{ij})_\mu$. The result of this multiplication of the order parameter at site i is then the value of the order parameter at the site

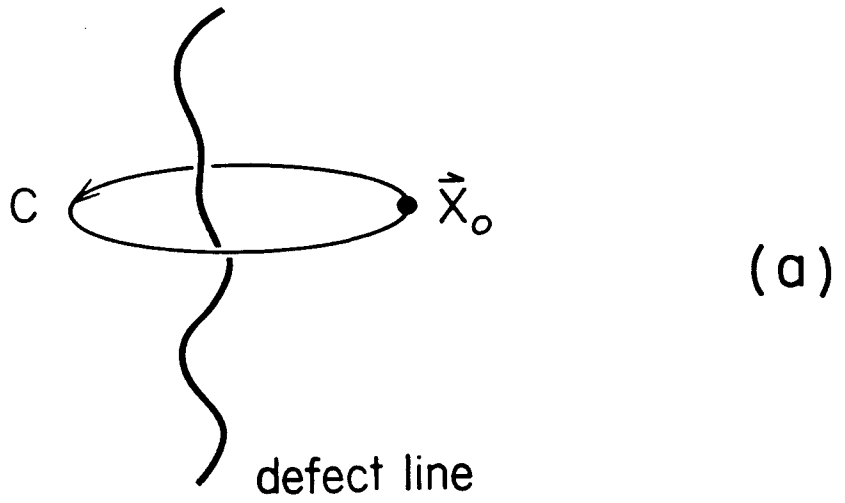

(a)

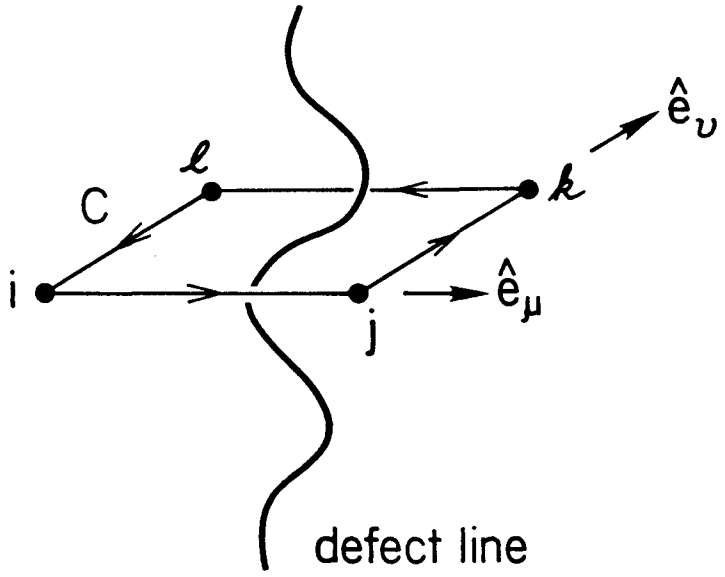

(b)

Figure A2.1 a) A closed plane curve C which surrounds a line defect in the predominantly icosahedral material. b) A discretized version of the closed plane curve C. The order parameter is defined on the sites i, j, etc., and the frustration field transporters, U_{ij}, etc., exist on the line segments between sites.

j. Upon traversing the loop, the net change in the order parameter is (see Figure A2.1(b)),

$$Q_{12,m_1m_2}(\vec{x}_0) \overset{\text{Traverse C}}{\longrightarrow} (U_{li})_{-\nu}(U_{kl})_{-\mu}(U_{jk})_{\nu}(U_{ij})_{\mu}\, Q_{12,m_1m_2}(\vec{x}_0) \qquad \text{(A2.4)}$$

In analogy with the gauge theory of electromagnetism, each transporter can be written as the exponential of a vector potential, which we shall call $\vec{A}$;

$$(U_{ij})_{\mu} \equiv e^{iA_{\mu}(x_{ij})a} \qquad \text{(A2.5)}$$

where x_{ij} is a representative point somewhere on the line between i and j, and a is the distance between i and j. The change in the order parameter can then be written as;

$$Q_{12,m_1m_2}(\vec{x}_0) \overset{\text{Traverse C}}{\longrightarrow} e^{i\oint_C \vec{A}\cdot d\vec{l}}\, Q_{12,m_1m_2}(\vec{x}_0) \qquad \text{(A2.6)}$$

By Gauss' theorem, the circulation of the potential $\vec{A}$ around the loop C is associated with the flux of a field, which we call the "disorder field," through the loop.

$$Q_{12,m_1m_2}(\vec{x}_0) \overset{\text{Traverse C}}{\longrightarrow} e^{i(\text{flux of disorder field through C})} Q_{12,m_1m_2}(\vec{x}_0)$$

From studying the defect algebra of the icosahedral order parameter, we know that the change in the order parameter upon circulating in a loop is an element of the group $Y' \times Y'$;

$$Q_{12,m_1m_2}(\vec{x}_0) \overset{\text{Traverse C}}{\longrightarrow} g\, Q_{12,m_1m_2}(\vec{x}_0) \qquad \text{where } g \in Y' \times Y' \qquad \text{(A2.7)}$$

From Equation (A2.4) we see that this group element g is the result of a product of transporters, U_{ij}, etc. Since these transporters must be closed under multiplication, have an inverse ($(U_{ij})_{\mu}^{-1} = (U_{ji})_{-\mu}$) which is also a transporter, have an identity element, and obey an associative law, they too are elements of the group $Y' \times Y'$.

We have now replaced the icosahedral order parameter defect lines with a disorder field and its associated transporters. The field theory of icosahedral metallic glass now consists of two parts:

1. An icosahedral order parameter field $Q_{12,m_1m_2}(\vec{x})$ (with a symmetry group SO(4)/G) defined on atomic sites in the glass,
2. A disorder field, represented by order parameter transporters U (which are elements of the group $Y' \times Y'$) between the atomic sites.

This formulation of icosahedral metallic glass structure is now very similar in form to gauge field theories of strongly interacting elementary particles [Creutz, 1983; Rebbi, 1983]. In these field theories, the order parameter represents the state of the particle (chosen from a manifold of states) at a given point in space-time. The gauge field acts to rotate the order parameter as it is moved through space. The strengths of the coupling between the order parameter and the external field and between order parameters on neighboring sites determines the equilibrium properties of the system.

A2.4 Gauge Theories and the Free Energy Functional

Local gauge invarisystem.

A2.4 Gauge Theories and the Free Energy Functional

Local gauge invariance is a demand made upon a theory that the description of a state (e.g., whether a spin is "up" or "down") be chosen independently at each point in space-time [Moriyasu, 1983]. Local gauge invariance allows us to choose arbitrarily which direction is "up" at each point in space without reference to any other point. The rule for comparing choices at different locations is provided by the "connection." In our theory of predominantly icosahedral materials, disorder invariance means that all physical expressions must be invariant under local changes of the line defect group parameterization. The line defect parameterization group now acts as our gauge group. In a gauge theory, one has a matter field (analogous to the icosahedral order parameter) and a gauge field (analogous to the disorder field) to provide a connection between sites where the matter field is defined.

Toulouse [Toulouse, 1977] developed the idea that local frustration can be introduced into a theory of glasses with the aid of a gauge field. Several authors have previously proposed gauge theories of metallic glass structure. Rivier and Duffy [Rivier and Duffy, 1982] proposed a gauge theory of glass based on the gauge group Z_2. Kleinert [Kleinert, 1984] modeled the glassy state by introducing quenched random disorder into the low-temperature phase of his gauge theory of dislocation melting. These two theories suffer from an overly simplified description of the defects that one expects to find in a real metal. Neither of these theories started from the basic assumption that frustrated icosahedral local ordering is responsible for the global disorder of the material. Hence the defects (and the gauge groups) used in these theories are oversimplified, leading to an incomplete description of a metallic glass. Our work differs from these primarily in that the gauge group is different, hence our description of icosahedral order and defects are novel. For a review of work on gauge theories of glasses, see the paper by Venkataraman and Sahoo [Venkataraman and Sahoo, 1986].

We can proceed to construct a gauge theory analogy for the theory of icosahedral metallic glass by using the analogy with one of the simplest gauge theories; the Ginzburg-Landau (GL) theory of superconductivity [Anlage, 1987] (see Figure 5.1). In the GL theory, the order parameter is the complex scalar electron condensate wave function ψ. The external field, which is coupled to the condensate, is the applied magnetic field $\vec{H}$. The free energy functional for a superconductor with condensate wave function ψ in an external field $\vec{H}$ is [Tinkham, 1975],

$$F = \frac{1}{2m^*}|(-i\hbar\nabla - \frac{e^*}{c}\vec{A})\psi|^2 + \alpha|\psi|^2 + \frac{|\vec{H}|^2}{8\pi} + \gamma|\psi|^3 + \frac{1}{2}\beta|\psi|^4 + \ldots \quad \text{(A2.8)}$$

where m^* and e^* are the effective mass and charge of the condensate particles, $\vec{A}$ is the vector potential associated with the field $\vec{H}$, and α, β, γ are temperature dependent parameters. Note that this expression is invariant under the global phase change $\psi \rightarrow \psi e^{-i\phi}$. The order parameter space is a unit circle in the complex

plane. Using homotopy theory [Mermin, 1979], one finds that the gauge group of the condensate wave function is Z (e.g., the group of integers under addition). This is the gauge group of the magnetic flux quanta in the bulk superconductor.

The first term of Equation (A2.8) represents the kinetic energy of the condensate and contains the covariant derivative for a charge moving in the presence of an external electromagnetic field. This term is invariant (in a stronger sense than above) under the spatially dependent substitution $\psi \rightarrow \psi e^{-i\phi(\vec{x})}$, providing $\vec{A} \rightarrow \vec{A} - \frac{\hbar c}{e}\nabla\phi$. The fact that the free energy is invariant under this dual transformation means that the order parameter has a "hidden" gauge symmetry. The second and third terms of Equation (A2.8) represent the self energy of the condensate and the external magnetic field respectively.

In Table 5.1 we present a detailed analogy between the GL theory of superconductivity and the gauge field theory of predominantly icosahedral materials. The free energy expansion analogous to Equation (A2.8) for an icosahedral metallic glass in terms of the icosahedral order parameter is;

$$\begin{aligned} F \;=\; & \frac{K}{2}\sum_{m} |D_\mu\, Q_{12,m}|^2 \;+\; \alpha \sum_{m} |\, Q_{12,m}\,|^2 \;+ \\ & \frac{1}{3}|F_{\mu\nu}|^2 \;+\; \text{SO(4) invariant higher order terms,} \end{aligned} \tag{A2.9}$$

where K and α are elastic constants and m stands for the pair (m_1, m_2). The covariant derivative in the first term is,

$$D_\mu Q_{12,m} \;=\; \sum_{m'} [\; \delta_{m,m'}\partial_\mu - i\kappa\, (A_\mu)_{m,m'} \;]\; Q_{12,m'}, \tag{A2.10}$$

where κ is a coupling constant between the order parameter and disorder fields, and the vector potential is,

$$(A_\mu)_{m,m'} \;\equiv\; \sum_{\alpha\,=\,1}^{6} \partial_\mu\, \theta_\alpha(\vec{r})\; (L_\alpha^{(12)})_{m,m'}. \tag{A2.11}$$

The $\theta_\alpha(\vec{r})$ are spatially dependent Lie angles and the $L_\alpha^{(12)}$ are the six SO(4) generators which are required to perform all possible rotations on the order parameter.

The *Lie angles* simply specify the spatial variation of the local gauge (or disorder) parameterization. The covariant derivative is, by definition, unchanged under a transformation of the gauge (or disorder) parameterization in the model.

The second and higher order terms in Equation (A2.9) represent the energy of the icosahedral order parameter field. The third term involves the disorder field tensor;

$$F_{\mu\nu} \equiv \partial_\mu A_\nu - \partial_\nu A_\mu - i\kappa[A_\mu, A_\nu], \qquad \text{(A2.12)}$$

and represents the self energy of the disorder field. The combination algebra (given by the group $Y' \times Y'$) of the line defects in this icosahedral medium is non-Abelian, i.e., the result of combining two line defects depends on the order in which they are combined. This means that defect lines often will not pass freely through one another (i.e., upon crossing they may develop an umbilical line), hence the disorder field tensor (Equation (A2.12)) will have a non-zero commutator. Higher order terms in Equation (A2.9) must be invariant under the operations of SO(4) since the total free energy functional should not depend on the details of how the tangent sphere S^3 is oriented to calculate the icosahedral order parameter (A2.2).

The free energy functional (A2.9) has several sensible physical properties. High defect line concentrations are discouraged by the presence of the disorder field tensor term (analogous to $H^2/8\pi$ term in the Ginzburg-Landau theory of superconductivity, Equation (A2.8)). Also, parallel icosahedral order parameters on neighboring sites are encouraged by the second term in Equation (A2.9). This will insure the presence of long range orientational order at low temperatures. Finally, the covariant derivative ensures that the order parameter field does not change its value on very short length scales.

REFERENCES

Chapter 1

Anlage, S. M., Cotts, E. J., Johnson, W. L., Follstaedt, D. M. and Knapp, J. A. (1987), in preparation.

Bak, P. (1986) Phys. Rev. Lett. 56, 861.

Ball, M. D. and Lloyd, D. J. (1985) Scripta Met. 19, 1065.

Bancel, P. A., Heiney, P. A., Stephens, P. W., Goldman, A. I. and Horn, P. M. (1985) Phys. Rev. Lett. 54, 2422.

Bancel, P. A. and Heiney, P. A. (1986) J. Phys. (Paris) 47, C3-341.

Bendersky, L. and Kaufman, M. (1986) Phil. Mag. Letts. 53, L75.

Bergman, G., Waugh, J. L. T. and Pauling, L. (1957) Acta Cryst. 10, 254.

Bernal, J. D. (1965) Liquids : Structure, Properties, Solid Interactions, ed. by Hughel, T. J. (Elsevier, Amsterdam), p. 25.

Briant, C. L. (1976) Discuss. Faraday Soc. 61, 25.

Briant, C. L. and Burton, J. J. (1978) Phys. Status Solidi B: 85, 393.

Burns, G. (1985) Solid State Physics (Academic Press, Orlando), p. 46.

Cassada, W. A., Shen, Y., Poon S. J. and Shiflet, G. J. (1986) Phys. Rev. B 34, 7413.

Dong, C., Hei, Z. K., Wang, L. B., Song, Q. H., Wu, Y. K. and Kuo, K. H. (1986) Scripta Met. 20, 1155.

Elser, V. (1986) Acta Cryst. A 42, 36.

Farges, J. (1973) J. Chem. Phys. 59, 3454.

Frank, F. C. (1952) Proc. Roy. Soc. 215, 43.

Hafner, J. (1982) J. Phys. F 12, L205.

Hafner, J. (1985) J. Phys. (Paris) 46, C9-69.

Hamermesh, M. (1962) Group Theory and its Application to Physical Problems (Addison-Wesley, Reading, Mass.), p. 51.

Harris, I. A., Kidwell, R. S. and Northby, J. A. (1984) Phys. Rev. Lett. 53, 2390.

Hiraga, K., Hirabayashi, M., Inoue, A. and Masumoto, T. (1985) Sci. Rep. Res. Inst., Tohoku Univ. A32, 309.

Hoare, M. R. and Pal, P. (1971) Adv. Phys. 20, 161.

Hoare, M. (1976) Ann. N.Y. Acad. Sci. 279, 186.

Kittel, C. (1976) Introduction to Solid State Physics (J. Wiley, New York), p. 9.

Kléman, M. and Sadoc, J. F. (1979) J. Phys. Lett. (Paris) 40, L-569.

Kramer, P. and Neri, R. (1984) Acta Cryst. A 40, 580.

Kuo, K. H., Zhou, D. S. and Li, D. X. (1987) Phil. Mag. Lett. 55, 33.

Levine, D. and Steinhardt, P. J. (1984) Phys. Rev. Lett. 53, 2477.

Nelson, D. R. (1983a) Phys. Rev. Lett. 50, 982.

Nelson, D. R. (1983b) Phys. Rev. B 28, 5515.

Nelson, D. R. and Widom, M. (1984) Nucl. Phys. B 240, 113.

Pauling, L. (1960) The Nature of the Chemical Bond, 3rd ed. (Cornell University Press, Ithaca), p. 425.

Pauling, L. (1985) Nature 317, 512.

Pauling, L. (1987) Phys. Rev. Lett. 58, 365.

Perepezko, J. H. and Paik, J. S. (1984) J. Non-Cryst. Solids 61&62, 113.

Poon, S. J., Drehman, A. J. and Lawless, K. R. (1985) Phys. Rev. Lett. 55, 2324.

Ramachandrarao, P. and Sastry, G. V. S. (1985) Pramãna 25, L225.

Sachdev, S. and Nelson, D. R. (1984) Phys. Rev. Lett. 53, 1947.

Sachdev, S. and Nelson, D. R. (1985) Phys. Rev. B 32, 1480.

Sadoc, J. F. (1981) J. Non-Cryst. Solids 44, 1.

Samson, S. (1968) Structural Chemistry and Molecular Biology, ed. by Rich, A. (W. H. Freeman, San Francisco), p. 687.

Samson, S. (1969) Developments in the Structural Chemistry of Alloy Phases, ed. by Giessen, B. C. (Plenum, New York), p. 65.

Shechtman, D., Blech, I., Gratias, D. and Cahn, J. W. (1984) Phys. Rev. Lett. 53, 1951.

Shechtman, D. and Blech, I. (1985) Met. Trans. A 16, 1005.

Socolar, J. E. S., Steinhardt, P. J. and Levine, D. (1985) Phys. Rev. B 32, 5547.

Steinhardt, P. J., Nelson, D. R. and Ronchetti, M. (1981) Phys. Rev. Lett. 47, 1297.

Steinhardt, P. J., Nelson, D. R. and Ronchetti, M. (1983) Phys. Rev. B 28, 784.

Stephens, P. W. and Goldman, A. I. (1986) Phys. Rev. Lett. 56, 1168.

Toulouse, G. (1977) Commun. Phys. 2, 115.

Turnbull, D. (1950) J. Metals, Trans. A.I.M.E. 188, 1144.

Ubbelohde, A. R. (1965) Melting and Crystal Structure (Clarendon Press, Oxford), p. 342.

Walford, L. K. (1964) Acta Cryst. 17, 57.

Weyl, H. (1952) Symmetry (Princeton University Press, Princeton), p. 73.

Zallen, R. (1983) The Physics of Amorphous Solids (Wiley, New York), p. 58.

Zhang, Z., Ye, H. Q. and Kuo, K. H. (1985) Phil. Mag. A 52, L49.

Chapter 2

Anlage, S. M., Fultz, B. and Krishnan, K. M. (1987a), submitted to J. Mater. Res.

Anlage, S. M. and Schwarz, R. B. (1987b), in preparation.

Anlage, S. M., Cotts, E. J., Johnson, W. L., Follstaedt, D. M. and Knapp, J. A. (1987c), in preparation.

Bancel, P. A., Heiney, P. A., Stephens, P. W., Goldman, A. I. and Horn, P. M. (1985) Phys. Rev. Lett. 54, 2422.

Klement Jr., W., Willens, R. H. and Duwez, P. (1960) Nature 187, 869.

Kroeger, D. M., Coghlan, W. A., Easton, D. S., Koch, C. C. and Scarbrough, J. O. (1982) J. Appl. Phys. 53, 1445.

Mehra, M. (1984) Ph.D. Thesis, Caltech.

Pietrokowsky, P. (1963) Rev. Sci. Instrum. 34, 445.

Schwarz, R. B., Petrich, R. R. and Saw, C. K. (1985) J. Non-Cryst. Solids 76, 281.

Taylor, M. A. (1960) Acta Met. 8, 256.

Chapter 3

Anlage, S. M., Nash, P., Ramachandran, R. and Schwarz, R. B. (1987) J. Less Common Metals.

Bendersky, L., Schaefer, R. J., Biancaniello, F. S., Boettinger, W. J., Kaufman, M. J. and Shechtman, D. (1985a) Scripta Met. 19, 909.

Bendersky, L. (1985b) Phys. Rev. Lett. 55, 1461.

Bendersky, L. A. and Ridder, S. D. (1986) J. Mater. Res. 1, 405.

Edshammar, L. (1968) Acta Chem. Scand. 22, 2374.

Edshammar, L. (1965) Acta Chem. Scand. 19, 2124.

Follstaedt, D. M. and Knapp, J. A. (1987a) Nucl. Inst. Meth. B 19, 611.

Follstaedt, D. M. and Knapp, J. A. (1987b) J. Mater. Sci. 90, to be published.

Knapp, J. A. and Follstaedt, D. M. (1987a) Phys. Rev. Lett. 58, 2454.

Knapp, J. A. and Follstaedt, D. M. (1987b), private communication.

Krishnan, K. M., Gronsky, R. and Tanner, L. E. (1986) Scripta Met. 20, 239.

Kroeger, D. M., Coghlan, W. A., Easton, D. S., Koch, C. C. and Scarbrough, J. O. (1982) J. Appl. Phys. 53, 1445.

Perepezko, J. H. and Boettinger, W. J. (1983) Mat. Res. Soc. Symp. Proc. 19, 223, ed. by L. H. Bennett, T. B. Massalski and B. C. Giessen.

Schaefer, R. J. (1986) Scripta Met. 20, 1187.

Shechtman, D., Blech, I., Gratias, D. and Cahn, J. W. (1984) Phys. Rev. Lett. 53, 1951.

Varich, A. N. and Lyukevich, R. B. (1973) Akad. Nauk. SSSR Izvest. Met., Eng. Trans. 1, 73.

Chapter 4

Anlage, S. M. (1987) Proceedings of the International Workshop on Quasicrystals (ed. by K. H. Kuo), Trans Tech., Switzerland, to be published.

Coxeter, H. S. M. (1973) Regular Polytopes (Dover, New York).

Frank, F. C. and Kasper, J. S. (1958) Acta Cryst. 11, 184.

Frank, F. C. and Kasper, J. S. (1959) Acta Cryst. 12, 483.

Nelson, D. R. and Toner, J. (1981) Phys. Rev. B 24, 363.

Nelson, D. R. (1983a) Phys. Rev. Lett. 50, 982.

Nelson, D. R. (1983b) Phys. Rev. B 28, 5515.

Nelson, D. R. and Widom, M. (1984) Nucl. Phys. B 240, 113.

Sinha, A. K. (1972) Prog. Mat. Sci. 15, 79.

Steinhardt, P. J., Nelson, D. R. and Ronchetti, M. (1981) Phys. Rev. Lett. 47, 1297.

Steinhardt, P. J., Nelson, D. R. and Ronchetti, M. (1983) Phys. Rev. B 28, 784.

Chapter 5

Nelson, D. R. (1983a) Phys. Rev. Lett. 50, 982.

Nelson, D. R. (1983b) Phys. Rev. B 28, 5515.

Nelson, D. R. and Widom, M. (1984) Nucl. Phys. B 240, 113.

Rebbi, C. (1983) Lattice Gauge Theories and Monte Carlo Simulations (World Scientific, Singapore).

Rose-Innes, A. C. and Rhoderick, E. H. (1978) Introduction to Superconductivity (Pergamon, Oxford), p. 183.

Tinkham, M. (1975) Introduction to Superconductivity (McGraw-Hill, New York), p. 104.

Wilson, K. (1974) Phys. Rev. D 10, 2445.

Chapter 6

Anlage, S. M., Fultz, B. and Krishnan, K. M. (1987), submitted to J. Mater. Res.

Swalin, R. A. (1962) Thermodynamics of Solids (Wiley, New York), p. 77.

Appendix I

Burns, G. (1985) Solid State Physics (Academic Press, Orlando), p. 46.

Frank, F. C. (1952) Proc. Roy. Soc. 215, 43.

Hamermesh, M. (1962) Group Theory and its Application to Physical Problems (Addison-Wesley, Reading, Mass.), p. 51.

Kittel, C. (1976) Introduction to Solid State Physics (J. Wiley, New York), p. 9.

Kléman, M. and Sadoc, J. F. (1979) J. Phys. Lett. (Paris) 40, L-569.

Sadoc, J. F. (1981) J. Non-Cryst. Solids 44, 1.

Venkataraman, G. and Sahoo, D. (1985) Contemp. Phys. 26, 579.

Appendix II

Anlage, S. M. (1987) Proceedings of the International Workshop on Quasicrystals (ed. by K. H. Kuo), Trans Tech., Switzerland, to be published.

Bernal, J. D. (1965) Liquids : Structure, Properties, Solid Interactions, ed. by Hughel, T. J. (Elsevier, Amsterdam), p. 25.

Creutz, M. (1983) Quarks, Gluons and Lattices (Cambridge, New York).

Frank, F. C. and Kasper, J. S. (1958) Acta Cryst. 11, 184.

Frank, F. C. and Kasper, J. S. (1959) Acta Cryst. 12, 483.

Kleinert, H. (1984) Phys. Lett. A 101, 224.

Kléman, M. (1977) J. Phys. Lett. (Paris) 38, L-199.

Mermin, N. D. (1979) Rev. Mod. Phys. 51, 591.

Moriyasu, K. (1983) An Elementary Primer for Gauge Theory (World Scientific, Singapore).

Nelson, D. R. (1983) Phys. Rev. B 28, 5515.

Nelson, D. R. and Widom, M. (1984) Nucl. Phys. B 240, 113.

Rebbi, C. (1983) Lattice Gauge Theories and Monte Carlo Simulations (World Scientific, Singapore).

Rivier, N. and Duffy, D. M. (1982) J. Phys. (Paris) 43, 293.

Tinkham, M. (1975) Introduction to Superconductivity (McGraw-Hill, New York), p. 104.

Toulouse, G. and Kléman, M. (1976) J. Phys. Lett. (Paris) 37, L-149.

Toulouse, G. (1977) Commun. Phys. 2, 115.

Venkataraman, G. and Sahoo, D. (1986) Contemp. Phys. 27, 3.